NeuroImage: Clinical 26 (2020) 102242

Contents lists available at ScienceDirect

NeuroImage: Clinical

journal homepage: www.elsevier.com/locate/ynicl

Image acquisition and quality assurance in the Boston Adolescent Neuroimaging of Depression and Anxiety study

Viviana Siless[a,b], Nicholas A. Hubbard[c,d], Robert Jones[a,b], Jonathan Wang[a,b], Nicole Lo[c], Clemens C.C. Bauer[c,e], Mathias Goncalves[c], Isabelle Frosch[c], Daniel Norton[a,b], Genesis Vergara[f], Kristina Conroy[g], Flavia Vaz De Souza[h], Isabelle M. Rosso[f,b], Aleena Hay Wickham[g], Elizabeth Ann Cosby[f], Megan Pinaire[g], Dina Hirshfeld-Becker[h], Diego A. Pizzagalli[f], Aude Henin[h], Stefan G. Hofmann[g], Randy P. Auerbach[i], Satrajit Ghosh[b,c], John Gabrieli[c], Susan Whitfield-Gabrieli[c,e], Anastasia Yendiki[a,b,*]

[a] Athinoula A. Martinos Center for Biomedical Imaging, Department of Radiology, Massachusetts General Hospital, Boston, MA, United States
[b] Harvard Medical School, Boston, MA, United States
[c] Massachusetts Institute of Technology, Cambridge, MA, United States
[d] University of Nebraska, Lincoln, Lincoln, NE, United States
[e] Northeastern University, Department of Psychology, Boston, MA, United States
[f] McLean Hospital, Belmont, MA, United States
[g] Boston University, Boston, MA, United States
[h] Massachusetts General Hospital, Boston, MA, United States
[i] Columbia University, New York, NY, United States

ARTICLE INFO

Keywords:
Depression
Anxiety
HCP
RDoC
DSM-5
BANDA

ABSTRACT

The Connectomes Related to Human Diseases (CRHD) initiative was developed with the Human Connectome Project (HCP) to provide high-resolution, open-access, multi-modal MRI data to better understand the neural correlates of human disease. Here, we present an introduction to a CRHD project, the Boston Adolescent Neuroimaging of Depression and Anxiety (BANDA) study, which is collecting multimodal neuroimaging, clinical, and neuropsychological data from 225 adolescents (ages 14–17), 150 of whom are expected to have a diagnosis of depression and/or anxiety. Our transdiagnostic recruitment approach samples the full spectrum of depressed/anxious symptoms and their comorbidity, consistent with NIMH Research Domain Criteria (RDoC). We focused on an age range that is critical for brain development and for the onset of mental illness. This project sought to harmonize imaging sequences, hardware, and functional tasks with other HCP studies, although some changes were made to canonical HCP methods to accommodate our study population and questions. We present a thorough overview of our imaging sequences, hardware, and scanning protocol. We detail similarities and differences between this study and other HCP studies. We evaluate structural-, diffusion-, and functional-image-quality measures that may be influenced by clinical factors (e.g., disorder, symptomatology). Signal-to-noise and motion estimates from the first 140 adolescents suggest minimal influence of clinical factors on image quality. We anticipate enrollment of an additional 85 participants, most of whom are expected to have a diagnosis of anxiety and/or depression. Clinical and neuropsychological data from the first 140 participants are currently freely available through the National Institute of Mental Health Data Archive (NDA).

1. Introduction

Depression and anxiety are two of the most prevalent psychiatric conditions. Adolescents with these disorders are more likely to have negative outcomes later in life, including academic and social difficulties and suicide (Woodward et al., 2001; Fergusson et al., 2002). Evidence from neuroimaging suggests altered brain features in these adolescents compared to controls. Structural magnetic resonance imaging (MRI) has detected alterations to cortical thickness and subcortical volumes (MacMaster and Kusumakar, 2004; Ducharme et al., 2014;

* Corresponding author.
E-mail address: ayendiki@mgh.harvard.edu (A. Yendiki).

https://doi.org/10.1016/j.nicl.2020.102242
Received 13 November 2019; Received in revised form 19 February 2020; Accepted 10 March 2020
Available online 19 March 2020
2213-1582/ © 2020 The Authors. Published by Elsevier Inc. This is an open access article under the CC BY-NC-ND license (http://creativecommons.org/licenses/BY-NC-ND/4.0/).

Marrus et al., 2015; Schmaal et al., 2016). Functional MRI (fMRI) has shown altered activation in brain regions associated with cognitive, reward, and other systems (Thomas et al., 2001; Monk et al., 2006; McClure et al., 2007; Kerestes et al., 2013). Diffusion MRI (dMRI) has detected white matter microstructural abnormalities in prefrontal, limbic, and other pathways (Cullen et al., 2010; Henderson et al., 2013; LeWinn et al., 2014; Liao et al., 2014; Bracht et al., 2015).

Much of our knowledge regarding anxious or depressed adolescent brain changes has been derived from small brain imaging studies, each with a unique set of acquisition parameters and patient characteristics (Kerestes et al., 2013; Bracht et al., 2015). Many of these studies have provided critical and lasting insights contributing to our understanding of the neurodevelopment of these disorders. However, smaller and heterogeneous datasets limit statistical power and may be particularly problematic for the generalization of brain imaging findings in psychiatric populations, which are invariably characterized by symptomatic heterogeneity. Individual studies yield inconsistent findings, and few of them are confirmed by meta-analyses (Murphy et al., 2011; Chen et al., 2016). For instance, a recent meta-analysis spanning 99 individual functional imaging experiments that compared brain activations between depressed (N = 1058 patients) and control groups failed to yield a single reliable voxel-wise group effect (Müller et al., 2017). Large open-access studies are advantageous in providing a high degree of statistical power and enabling the broader scientific community to test a wide array of desired hypotheses. Additionally, standardized data acquisition, processing, and sharing allow for a higher degree of experimental control compared to non-standardized approaches, which is beneficial for the purposes of replication (Peng, 2011; Nichols et al., 2017).

Recent initiatives aimed at generating large, open-access brain imaging datasets have gained considerable popularity in healthy adults (Schumann et al., 2010; Van Essen et al., 2012), diseased populations (Weiner, 2010; di Martino et al., 2014), and aging (Bookheimer et al., 2019). Moreover, recent efforts have targeted understanding typical childhood and adolescent brain development through the lens of large and open-access neuroimaging initiatives such as the Adolescent Brain Cognitive Development study (ABCD) (Volkow et al., 2018), IMAGEN (Schumann et al., 2010), Philadelphia Neurodevelopmental Cohort (Satterthwaite et al., 2016), and the HCP lifespan development study (HCP-D) (Somerville et al., 2018). The HCP has provided the neuroimaging community with high-resolution MRI acquisition protocols, image pre-processing methods, and a large database managed by the Connectome Coordination Facility to facilitate the collection and dissemination of standardized and open-access brain imaging data. The HCP Young Adult (HCP-YA; Van Essen et al., 2012) study to date has produced meaningful and reliable findings on typical brain organization and has led to the development of useful brain imaging tools (see Glasser et al., 2016). The success of this initial HCP study has prompted other HCP-based initiatives aimed at examining brain changes associated with typical development and healthy aging (Somerville et al., 2018; Bookheimer et al., 2019), as well as brain changes associated with human diseases or predisposition for disease. This latter group of studies, termed Connectomes Related to Human Disease (CRHD; see https://www.humanconnectome.org/disease-studies), takes advantage of the HCP protocols and the potential for comparison to a large, normative data set (HCP-YA) to investigate the neural correlates of human disease.

Here, we describe the Boston Adolescent Neuroimaging of Depression and Anxiety project (BANDA), a CRHD study aimed at better understanding, predicting, and diagnosing adolescent depression and anxiety disorders. This project will collect multimodal neuroimaging, clinical, and neuropsychological data from 225 adolescents beginning at ages 14 to 17. From these adolescents, 180 will have a current diagnosis of anxiety and/or depression according to Diagnostic and Statistical Manual of Mental Disorders (DSM-5) definitions (APA, 2013). Participants will undergo follow-up clinical assessments at six months and one year post-imaging to allow for inquiries into the longitudinal prediction of symptom changes. Although anxiety and depression are often treated as separate disorders in brain imaging studies, pure cases of these disorders are not largely represented in the adolescent population (Clark et al., 1995; Krueger, 1999) and co-morbidity may serve as a useful indicator of illness severity (Lang et al., 2016). Our recruitment requires positive classification of anxiety and/or depression based on DSM-5 (APA, 2013). However, the breadth of continuous measures collected by the BANDA project will also afford researchers opportunities to investigate the neural correlates of the full spectrum of depressed/anxious symptomatology. This approach is consistent with NIMH research domain criteria (RDoC; see www.nimh.nih.gov/research/research-funded-by-nimh/rdoc/).

This is the first HCP study on adolescent psychiatric populations. It will allow for larger-scale verification of previous brain imaging findings, as well as standardized comparisons to other HCP data. We have worked to harmonize imaging protocols with the HCP-D study, which is collecting imaging and behavioral data from 1300+ healthy children, adolescents, and young adults (Somerville et al., 2018). We have also coordinated efforts with three other CRHD projects that are examining aspects of adult anxiety and depression. In total, BANDA and these partner CRHD projects aim to collect data from over 900 participants, most of whom will have primary symptoms of depression or anxiety disorders.

The present manuscript details the imaging acquisition protocol and provides image quality assessments from the BANDA project. Detailed information on the clinical and neuropsychological measures, sample characteristics, and preliminary task fMRI findings may be found in our companion paper (see Hubbard et al., 2020). These articles are timed with the initial public release of data from the first 140 participants; thus, they serve as introductions to the project, as well as methodological references for those seeking to use these data, either in isolation or combined with other HCP datasets.

2. Participating sites

This project is a collaboration between five sites. Recruitment, data sharing, and study management are handled by the McGovern Institute for Brain Research at the Massachusetts Institute of Technology (MIT). Clinical assessment and administration of neuropsychological measurements occurs at: 1) the Center for Anxiety and Related Disorders at Boston University (BU), 2) the Center for Depression, Anxiety, and Stress Research at McLean Hospital at Harvard Medical School (McLean) and 3) the Child Cognitive Behavioral Therapy Program at Massachusetts General Hospital and Harvard Medical School (MGH). Finally, MRI scanning and administration of cognitive measurements involving eye tracking are performed at the Athinoula A. Martinos Center for Biomedical Imaging at Massachusetts General Hospital and Harvard Medical School (Martinos Center).

For the cross-sectional component of the study, adolescents participate in two sessions: 1) clinical assessment and administration of the neuropsychological measurements and 2) MRI scanning. Fig. 1 shows the data acquisition pipeline. For the longitudinal component of the study, clinical data are collected at six months and one year after the scan.

3. Imaging session considerations and challenges

A key consideration in designing the present study was ensuring the comfort of our participants during scanning. Many of our adolescent participants are anxious or have attention-deficit/hyperactivity disorder. Thus, we assumed that many participants would have reservations about entering the magnet or difficulties remaining still for the duration of scanning. At the outset of this study, we implemented several strategies to maximize participant comfort during MRI acquisition and thus decrease the probability of attrition or motion-corrupted

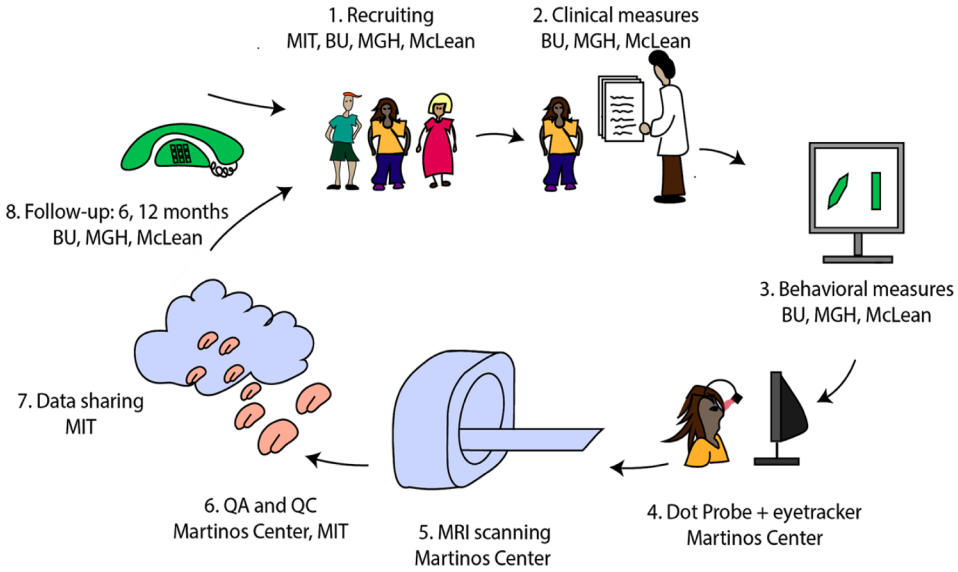

Fig. 1. Overview of events in the BANDA study.

data.

One way in which we tried to maximize participant comfort is by using a 64-channel coil (head: 7.75 × 9 × 9–10.5 in, eyes: 2.25 × 2.25–2.75 in), which is larger than the 32-channel coil (head: 7.75 × 9 × 9 in, eyes: 2.25 × 2 in) available for the scanner used in this study. The 64-channel coil has an ergonomic design and its position is fixed by connecting its posterior components directly to the gurney of the scanner, whereas the 32-channel coil connects through cables. Another strategy for maximizing participant comfort and compliance is by familiarizing participants with the scanning procedure during a mock-scanning session. This was done either at a mock scanner or an actual MR environment. In this session, participants received detailed explanations on what is expected from them during the scan and were instructed on the use of the button box and the emergency squeeze ball. We allowed participants to sleep or view nature videos during structural and dMRI scans.

We did not require any form of a medication "washout" period before scanning, with participant comfort and safety in mind. Information regarding medication usage was collected and will be made publicly available. Briefly, 51.7% of patients were taking some form of psychiatric medication (depressed 41.7%, anxious 63.4%). Records of medication types and status of all participants were collected and may be used as covariates in analyses. This is detailed in our companion manuscript, along with illicit and legal substance use in these participants (Hubbard et al., 2020).

A final way in which we attempted to maximize participant comfort is by minimizing scanning burden. Choices were made to reduce the number of fMRI tasks and only include those highly relevant to these disorders (see Hubbard et al., 2020). This meant omitting tasks collected by the HCP-YA study that probe constructs that may be relevant to general adolescent development (e.g., working memory or language tasks), but that might not be the most relevant for understanding adolescent depression and anxiety. Moreover, the functional tasks were parsed into short (3–6 min) runs to create multiple opportunities for rest breaks and "check-ins" from MRI operators. Resting state fMRI (rfMRI) scans, where participants had to fixate on a cross-hair, were alternated with dMRI scans, in which participants could watch nature videos, because during our piloting stage, even adult participants reported difficulty staying awake or fixating on the cross-hairs at the center of the screen for long periods of time.

The final imaging protocol is 1 h 36 min long, with a mean in-scanner time of 2 h and a standard deviation of 17 min. Table 1 shows the scans and their duration. This is longer than single sessions of other large-scale imaging studies with adolescent participants (Casey et al., 2018; Harms et al., 2018). Despite higher putative participant burden for a single session, about 80% of our participants reported feeling "good" or "very good" after scanning (6.58 mean and 1.93 standard deviation, with a score of 0 reflecting feeling "very bad" and a score of 10 reflecting feeling "very good"; see Fig. 2). This is also evidenced by the low attrition rate. Only one out of 140 participants requested to drop out of the study in the middle of the scanning session (0.71%), while 3 participants dropped out before entering the MRI (2.14%), and 2 dropped out after their initial clinical appointment (1.43%). The remaining participants completed the full scan session.

The steps that are taken to enhance participant comfort are presumed to also reduce motion-related confounds. However, other strategies are also employed to help reduce motion artifacts in these data. For T1- and T2-weighted scans, we use sequences with volumetric navigators and reacquisition for online monitoring and reduction of motion artifacts (Tisdall et al., 2012). During dMRI and fMRI acquisition, MRI operators are instructed to evaluate potential motion artifacts visually after each scan and give feedback to the participant. Since the onset of this project, advances have been made in monitoring head motion during echo-planar imaging (EPI) scans in real-time (Dosenbach et al., 2017). This method was adopted by the HCP-D study (Harms et al., 2018; Somerville et al., 2018) after we had scanned a considerable number of participants, thus we opted not to include it in our protocol.

3.1. Between-study harmonization

One goal of the BANDA project was to harmonize MRI acquisition with other HCP studies. Harmonization will facilitate cross-validation of findings from our sample, as well as combined hypothesis testing (see Harms et al., 2018). Our primary targets for harmonization were the HCP-D study of healthy childhood and adolescent development (see Harms et al., 2018; Somerville et al., 2018) and three CRHD studies: the Dimensional Connectomics of Anxious Misery (CRHD-AA), which aims to collect data from 200 adult participants with anxiety symptoms; the Perturbation of the Treatment of Resistant Depression Connectome by Fast-Acting Therapies (CRHD-DT), which aims to collect data from 200 adult participants with severe depression; and the Mapping Connectomes for Disordered Mental States (CRHD-DMS), which aims to collect data from 300 adult participants who are experiencing varying degrees of psychopathology (see humanconnectome.org/disease-studies/).

Table 1
BANDA acquisition protocol. Duration for T1w and T2w reflects the total time with the maximum allowed k-space re-acquisition. AP = anterior to posterior phase encoding (PE) direction; PA = posterior to anterior PE direction.

	Modality	PE	Resolution (mm)	Volumes	Duration	Stimulus
1	Localizer		.5×.5 × 7	–	0:12	Movie
2	AAHeadScout		1.6×1.6×1.6	–	0:14	Movie
3	T1w vNav setter		8 × 8 × 8	–	0:02	Movie
4	T2w vNav setter		8 × 8 × 8	–	0:02	Movie
5	T1w		.8×.8×.8	1	7:50	Movie
6	dMRI	AP	1.5 × 1.5 × 1.5	98	5:37	Movie
7		PA	1.5 × 1.5 × 1.5	98	5:37	Movie
8	Spin Echo	AP	2 × 2 × 2	3	0:32	Green screen
9		PA	2 × 2 × 2	3	0:32	Green screen
10	Resting-state fMRI	AP	2 × 2 × 2	420	5:46	Fixation
11		PA	2 × 2 × 2	420	5:46	Fixation
12	dMRI	AP	1.5 × 1.5 × 1.5	99	5:41	Movie
13		PA	1.5 × 1.5 × 1.5	99	5:41	Movie
14	Spin Echo	AP	2 × 2 × 2	3	0:32	Green screen
15		PA	2 × 2 × 2	3	0:32	Green screen
16	Resting-state fMRI	AP	2 × 2 × 2	420	5:46	Fixation
17		PA	2 × 2 × 2	420	5:46	Fixation
18	IPT fMRI	AP	2 × 2 × 2	215	3:02	IPT
19		PA	2 × 2 × 2	215	3:02	IPT
20	Spin Echo	AP	2 × 2 × 2	3	0:32	Green screen
21		PA	2 × 2 × 2	3	0:32	Green screen
22	EPT fMRI	AP	2 × 2 × 2	405	5:34	EPT
23		PA	2 × 2 × 2	405	5:34	EPT
24	EIT fMRI	AP	2 × 2 × 2	280	3:54	EIT
25		PA	2 × 2 × 2	280	3:54	EIT
26		AP	2 × 2 × 2	280	3:54	EIT
27		PA	2 × 2 × 2	280	3:54	EIT
28	T2w		.8×.8×.8	1	6:58	Movie

For this purpose, we use the same sequences as the aforementioned HCP studies. Table 2 lists similarities and differences between our scanning protocol, the HCP-YA, and the HCP-D. Our protocol for dMRI and fMRI is harmonized with the HCP-D. Different head coils are used (64-channel vs. 32-channel). Our structural T1- and T2-weighted images are harmonized with the HCP-YA, except for the incorporation of volumetric navigators for prospective motion correction, and thus differs from the HCP-D, which incorporated a multi-echo MPRAGE sequence (Harms et al., 2018). Scanners, duration of resting fMRI scans, and the gradient directions and b-values of dMRI scans are harmonized between our study and the CRHD-AA and CRHD-DT protocols. Each of our sister CRHD projects has at least one functional task similar to ours (see Table 3). The CRHD-DMS project acquires data using a scanner of a different manufacturer (GE). Acquisition parameters are very similar

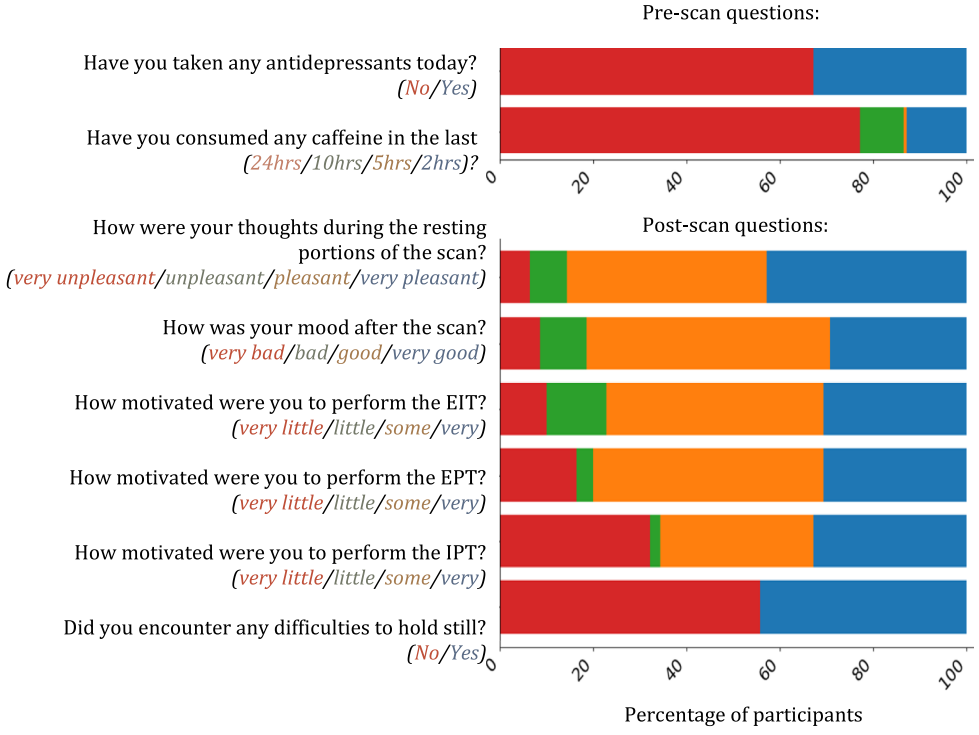

Fig. 2. Answers to selected questions from the pre- and post-scan questionnaires. Colors represent possible answers in order.

Table 2
Hardware and acquisition parameters for HCP-YA, HCP-D, BANDA and relevant CHRD projects.

	HCP-YA	HCP-D	BANDA	CRHD-AA	CRHD-DT	CRHD-DMS
Number of MRI acquisition sites	1	4	1	1	1	1
Scanner	Siemens Connectom 3T	Siemens Prisma 3T	Siemens Prisma 3T	Siemens Prisma 3T	Siemens Prisma 3T	GE Discovery MR750 3T
Head coil elements	32	32	64 (52 used)	64 (52 used)	32	32
Max. gradient strength (mT/m)	100	80	80	80	80	50
Structural images						
Resolution(mm)	.7 × .7 × .7	.8 × .8 × .8	.8 × .8 × .8	.8 × .8 × .8	.8 × .8 × .8	.8 × .8 × .8
FoV (mm)	244 × 244 × 180	256 × 240 × 167	256 × 240 × 167	256 × 240 × 167	256 × 240 × 167	256 × 256 × 184
T1w						
TE (ms)	2.14	1.81/3.6/5.39/7.18	2.18	2.22	1.81/3.6/5.39/7.18	3.548
TR (ms)	2400	2500	2400	2400	2500	2840
TI (ms)	1000	1000	1040	1000	1000	1060
Partial Fourier		6/8			slice 6/8	
Slice oversampling (%)	0	7.7	23.1	23.1	7.7	0
Max. vNav reacquisition	–	30	24	–	30	PROMO
Bandwidth (Hz/px)	210	740	220	220	740	122
Parallel imaging	2	2	2	2	2	2 × 1.25
Flip angle	8	8	8	8	8	8
Fat suppr.	water excitation	water excitation	water excitation	water excitation	water excitation	–
T2w						
TE (ms)	565	564	564	563	564	~75 (subject-specific)
TR (ms)	3200	3200	3200	3200	3200	2500
Slice oversampling (%)	0	7.7	0	0	7.7	0
Max. vNav reacquisition	–	25	18		25	PROMO
Bandwidth (Hz/Px)	744	744	744	744	744	488
Parallel imaging	2	2	2	2	2	1.9 × 1.9
EPI						
PE direction	LR/RL	AP/PA	AP/PA	AP/PA	AP/PA	AP/PA
dMRI						
b-values (s/mm^2)	1000/2000/3000	1500/3000	1500/3000	1500/3000	1500/3000	1500/3000
Diffusion directions by shell	89/90/91	92/93	92/93	92/93	92/93	74/76
Multiband factor	3	4	4	4	4	4
TR (ms)	5520	3230	3230	3230	3230	3200
TE (ms)	89.5	89.2	89.2	89.2	89.2	80
Resolution (mm)	1.25 × 1.25 × 1.25	1.5 × 1.5 × 1.5	1.5 × 1.5 × 1.5	1.5 × 1.5 × 1 × 5	1.5 × 1.5 × 1.5	1.5 × 1.5 × 1.5
fMRI						
TR (ms)	720	800	800	800	800	710
TE (ms)	33.1	37	37	37	37	30
Multiband factor	8	8	8	8	8	6
Resolution(mm)	2 × 2 × 2	2 × 2 × 2	2 × 2 × 2	2 × 2 × 2	2 × 2 × 2	2.4 × 2.4 × 2.4

Table 3
Length of fMRI scans in HCP-YA, HCP-D, BANDA and relevant CRHDs projects. Each entry shows (number of frames per run) × (number of runs).

fMRI scan	HCP-YA frames	HCP-D frames	BANDA frames	CRHD-AA frames	CRHD-DT frames	CRHD-DMS frames
Resting state	1200 × 4	488 × 4	420 × 4	420 × 4	488 × 2	440 × 4
IPT	253 × 2	280 × 2	215 × 2	228 × 2	–	316 × 1
EPT	176 × 2	178 × 1	405 × 2	340 × 2	338 × 2	204 × 1
EIT	–	–	280 × 4	290 × 4	–	–

and post-processing strategies could be applied to mitigate any potential differences prior to joint analyses. In the discussion, we elaborate on such strategies.

3.2. Within-study consistency

We ensured that participants received identical oral and written instructions[1] during the mock scanning and MRI scanning sessions (see Supplementary Data). For mock scanning, the first 41 participants were taken to a mock-scanner room. Due to infrastructure changes at the imaging site, the rest of the participants were instead trained in an active MRI environment with a 1.5T or 3T magnet, depending on availability.

[1] We thank Dr. Randy Buckner for providing us with the MRI instructions of the pilot lifespan HCP study, which we adapted to our protocol.

Resting-state and task fMRI practice sessions are performed on a laptop. The participants go through the instructions and tasks using a scanner button box or laptop keyboard. During practice, a researcher monitors that participants are performing these tasks appropriately. For each task, participants are instructed that the task is automated, and if they miss a trial they should continue on to the next trial. Tasks are administered in the following order: (1) incentive processing task (IPT), (2) emotion processing task (EPT), (3) emotion interference task (EIT). If a participant fails to respond accurately to at least 50% of the practice trials, the practice task and its instructions are restarted. Otherwise, the researcher verifies that the participant is comfortable with the task instructions and then continues on with the next portion of the study.

During the mock scanning session and throughout the actual MRI session, participants are reminded about the importance of remaining still in the scanner. Before entering the bore of the magnet, participants are shown an emergency "squeeze ball" and reminded that they may use it to leave the scanner at any moment. They are informed about scanner noises and the importance of ensuring earplugs are properly secured. Participants are also shown the head coil and the 5-finger button box that they use during the task fMRI scans. Head coil mirrors are placed at the bottom of the participant's nose. The participant is landmarked at the eyebrows and placed into the bore of the scanner. While in the scanner, before each scan, participants are told if they need to remain awake or if they may rest or watch a movie. The movie shows animals in nature without violent scenes. Participants may opt out of watching the movie, in which case a green screen is shown.

Although we attempt to keep data acquisition as consistent as possible across participants, changes in software and hardware occur outside of our control. The scanner host computer's software was updated from VE11B to VE11C after the first 15 participants were scanned. As part of the CMRR-sequence license agreement (http://license.umn.edu/technologies/cmrr), sequences needed to be updated every 6 months during the project. After scanning the 178th participant, the gradient coil of the scanner was replaced due to water leaking. We do not anticipate that these changes would have major effects on these data, however, prospective users of these data should be aware that such changes had occurred. Further, we do not detect any change in signal-to-noise ratio (SNR) at any of these timepoints.

4. Brain imaging

4.1. Hardware

Participants are imaged using a Siemens 3T Prisma whole-body scanner with 80 mT/m gradients capable of a slew rate of 200 T/m/s. This high gradient strength is especially valuable for achieving high diffusion weighting with shorter echo times and thus higher SNR (Setsompop et al., 2013; Ugurbil et al., 2013). We use the standard Siemens Prisma 64-channel head coil, which contains 52 head and 12 neck elements. Only head elements were used in our protocol. Button boxes used for fMRI scans contain 5 buttons, one for each finger, and are custom made by the scanning site. Buttons corresponding to the participant's four fingers are adjacent, while the button corresponding to the thumb is at a lower position in the pad. Left- and right-hand button boxes mirror one another and only one is given to a participant based upon his or her reported lateral-hand dominance. Instructions and images presented during fMRI, and videos presented during the structural and dMRI scans, are projected with a Sharp LCD XG-C465X which is back-projected to a mirror mounted on the head coil.

4.2. Structural MRI

The field of view for all scans is positioned automatically using Siemens' AutoAlign feature (Van der Kouwe et al., 2005), then visually inspected and corrected by an operator to avoid aliasing. A magnetization-prepared rapid acquisition with gradient echo (MPRAGE) sequence (Mugler et al., 1990) is used for T1w and a variable-flip-angle turbo-spin echo (TSE) sequence (Mugler et al., 2000) is used for the T2w scan. We use variants of these sequences that utilize embedded volumetric navigators (vNavs) for prospective correction of within-scan motion (Tisdall et al., 2012). This has been shown to reduce biases in brain morphometric analyses (Reuter et al., 2015; Tisdall et al., 2016). All acquisition parameters are shown in Table 2. The maximum duration for the T1w image is 7:50 min and the minimum is 6:52 min when no re-acquisition is necessary. For the T2w image, the maximum duration allowed is 6:58 min and minimum is 6:01 min.

The vNavs are low-resolution, 3D echo-planar images with low flip-angles. These images are acquired in about 0.2 s, at every TR of the primary scan. The vNav is inserted after the inversion pulse of the T1w scan, and during the TR delay for contrast of the T2w scan waiting period. This procedure adds no time to the total scan duration. The vNavs are used to calculate motion between TRs in real time, which is fed back to update the image field-of-view position. Additionally, quantitative information about motion between TRs is used to help detect highly-corrupted k-space lines that need re-acquisition. When there is motion between TRs that is greater than half a voxel in size, re-acquisition is employed, which adds modestly to the duration of the T1w and T2w scans (Tisdall et al., 2012).

4.3. Echo-planar imaging (EPI)

Scans are acquired with a 2D multi-band (MB) gradient-recalled echo (GRE) echo-planar imaging (EPI) sequence. We use anterior-posterior (AP) and posterior-anterior (PA) phase encoding directions to harmonize with the HCP-D (Harms et al., 2018). The Siemens Prisma scanner used in both projects is capable of achieving a shorter echo-train length in the AP/PA direction, while the Siemens Connectome scanner may achieve a shorter echo-train length with left-right and right-left phase encoding direction, helping to decrease signal drop-out (Smith et al., 2013).

4.3.1. Diffusion MRI

Diffusion-weighted images are acquired with an MB acceleration factor of 4, a partial Fourier factor of 6/8, TR = 3230 ms, TE = 89.20 ms. These sequences result in 1.5 mm isotropic voxel size with whole-brain coverage, via 92 oblique-axial slices and a field of view (FoV) of 210 × 210 × 138 mm. During acquisition, q-space is densely sampled with 183 diffusion-weighting directions, each acquired with two phase encoding directions (PA-AP). During the 4 runs, directions are sampled of the whole sphere on 2 shells of $b = 1500 s/mm^2$ and 3000 s/mm^2. Shells are interleaved within each dMRI run and 28 $b = 0$ vol are interspersed uniformly across the four runs. Images are acquired over 4 runs for a total of 22:36 min.

4.3.2. Functional MRI

The fMRI data are acquired with an MB acceleration factor of 8, TR = 800, TE = 37 ms, and a flip angle of 52 deg. These sequences result in 2.0 mm isotropic voxel size with whole-brain coverage, via 72 oblique-axial slices and an FoV of 208 × 208 × 144 mm. Every fMRI run is paired with a run that has the opposite phase encoding direction (PA-AP). Spin echo images are also acquired in opposite phase encoding directions (PA-AP) to further correct for EPI distortions in rfMRI and task fMRI (tfMRI).

Instructions, scanner tasks, and in-scanner follow-up questions for fMRI are programmed in PsychoPy (Peirce, 2007, 2008). These scripts are publicly available at: https://github.com/BANDA-connect.

4.3.2.1. Resting-state fMRI. During rfMRI scanning, participants are shown a small, white fixation cross on a gray background. Participants are instructed to keep still, stay awake, and blink normally while the fixation cross is on the screen. After each of the four 5:46 min runs, follow-up questions appear on the screen. These

questions inquire about relevant experiences that the participants might have during that run (e.g., about sleepiness and mind wandering). Participants respond to these questions via the button boxes.

4.3.2.2. Task-based fMRI. Here, we briefly describe the fMRI tasks. Additional information supporting task selection can be found in Supplemental Table 1. For more details and preliminary results from these tasks, see our companion article (Hubbard et al., 2020).

- Incentive Processing Task (IPT): Participants are asked to guess whether a forthcoming number to appear on the screen will be greater or less than 5 in order to win or lose money. Participants receive additional payment for their correct guesses during this task. However, the number of trials in which participants can win or lose money is fixed. This task is adapted from Delgado and colleagues (Delgado et al., 2000) and similar versions are used by the HCP-YA, the HCP-D (Barch et al., 2013), the CRHD-AA, and the CRHD-DMS.[2]
- Emotion Processing Task (EPT): Participants decide which of two pictures (happy, angry, sad, fearful, neutral expressions, or objects) presented on the bottom of the display is identical to the single picture at the top of the display (Hariri et al., 2002; Barch et al., 2013). We used the Radboud (Langner et al., 2010) and NimStim (Tottenham et al., 2008) face databases and object stimuli consisted of fruits and vegetables (Chai et al., 2015). We added a sad stimulus after the first 17 participants to remain consistent with adolescent depression literature (Stuhrmann et al., 2011). This added 6 more trials to each block in each run. Similar versions of this task are used in the HCP-YA, HCP-D, and CRHD-DT[2].
- Emotion Interference Task (EIT): Participants are presented a pair of houses and a pair of faces (fearful or neutral), one arranged horizontally and one vertically. They are instructed to attend to one axis and determine whether elements on that axis are the same, while ignoring the other axis (Vuilleumier et al., 2001; Wojciulik et al., 1998; Fales et al., 2008b). This task is also administered in the CRHD-AA.

Fig. 3 shows example images of T1w, T2w, dMRI and fMRI. For dMRI, $b = 0$ images are shown. We show dMRI and fMRI images for each PE direction to illustrate EPI distortions.

5. Study participants, clinical, and neuropsychological measures

Detailed information on participant demographics, recruitment, and characterization can be found in our companion paper (Hubbard et al., 2020). Briefly, adolescents are between the ages of 14 and 17 at imaging, are fluent in English, and have a score of 85 or higher on the Wechsler Abbreviated Scale of Intelligence (WASI-II; Wechsler, 2011). Diagnoses of present and historical psychiatric disorders are given by trained researchers who are, or are under the supervision of, clinical psychologists. Diagnoses are based upon the DSM-5 (APA, 2013). For ease of visualization and discussion, participants here are grouped into one of three categories: Control Adolescent (CA) group, Anxious Adolescent (AA) group, or Depressed Adolescent (DA). CAs have no present psychiatric disorders, or historical diagnosis of anxiety or depression. AAs meet the DSM-5 criteria for at least one anxiety disorder but do not have a current depressive disorder. DAs meet the DSM-5 criteria for a current depressive disorder and may also have a present or historical diagnosis of anxiety disorders.

[2] These tasks were re-implemented in PsychoPy and adapted to our scanner's trigger, button boxes, projector and monitoring screens. Instructions, practice and assessment questions were added.

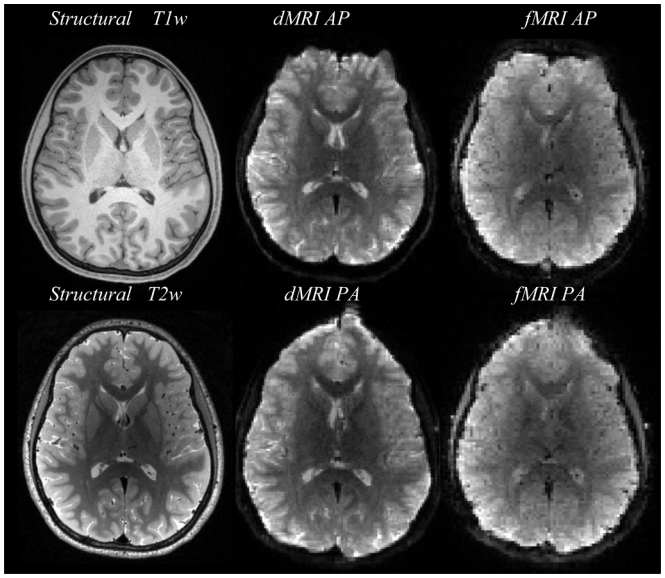

Fig. 3. Example images from a single participant.

5.1. Clinical dimensional measures

This project uses questionnaires to characterize key clinical dimensions related to adolescent anxiety and depression. A total of seven dimensional measures are collected for the BANDA project. These measures, as well as the reasoning behind their selection are discussed in our companion article (Hubbard et al., 2020). Here we assess the relationships between continuous clinical dimensions and measures of MRI quality. The following measures are presented because they provide a general summary of key clinical dimensions within our sample:

- **SHAPS:**The Snaith-Hamilton Pleasure Scale provides a dimensional measure of hedonic capacity and tone (Snaith et al., 1995). SHAPS scores greater than 2 are thought to reflect anhedonic tone. Administration takes ~5mins.
- **MFQ:**The Mood and Feelings Questionnaire (long version) is an assessment of core depressive symptoms (Angold et al., 1995). Administration takes ~7mins.
- **BIS-BAS:**The Behavioral Inhibition System and Behavioral Activation System questionnaire quantifies predisposition for "approach" (BAS) and "avoid" (BIS) behaviors (Carver et al., 1994). Administration takes ~3mins.

Fig. 4 demonstrates that groups show heterogeneous expressions of clinical dimensions. For instance, all groups are comprised of both anhedonic and non-anhedonic adolescents. The heterogeneity of diagnostic labels through clinical symptomatology suggests the importance of examining these disorders as continua.

5.2. Cognitive and neuropsychological measures

The cognitive and neuropsychological measures chosen for this project are largely consistent with the HCP-YA and HCP-D (Barch et al., 2013; Satterthwaite et al., 2016; Luciana et al., 2018). Measures are selected from the NIH toolbox (www.healthmeasures.net) and the University of Pennsylvania Computerized Neuropsychological Test Battery (Gur et al., 2001). The behavioral measures span a broad range in the domains of cognition, emotion, perception, and motor function. An additional measure of cognitive control in emotional contexts is

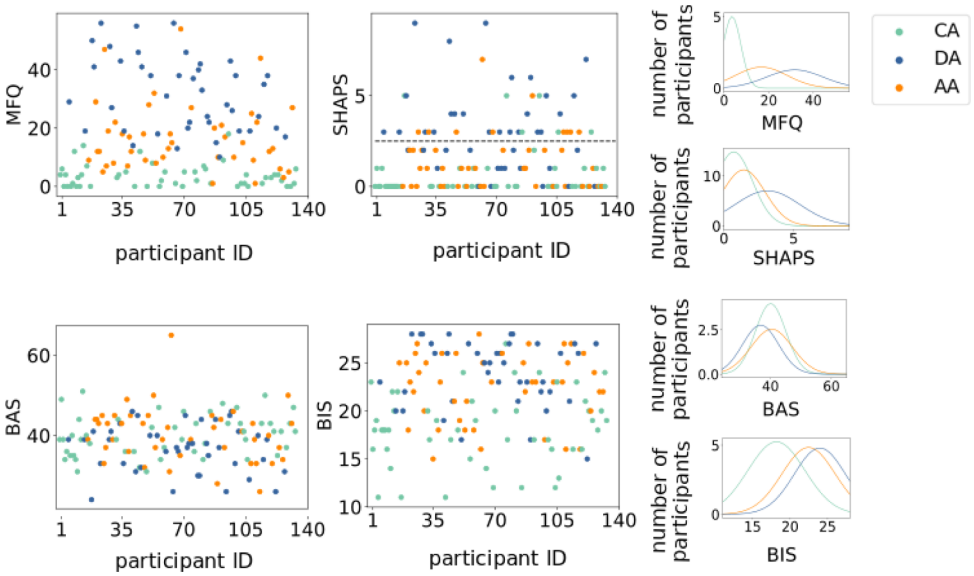

Fig. 4. Clinical variables: MFQ = Mood and Feelings Questionnaire score; SHAPS = Snaith-Hamilton Pleasure Scale (score greater than two reflects anhedonic symptomology); BAS = Behavior Activation Scale score; BIS = Behavioral Inhibition Scale score. CA = Control Adolescents; DA = Depressed Adolescents; AA = Anxious Adolescents. The first and second columns show scatter plots of each clinical variable for all participants, color-coded by group. The third column shows normal distributions fit to each clinical variable for each group.

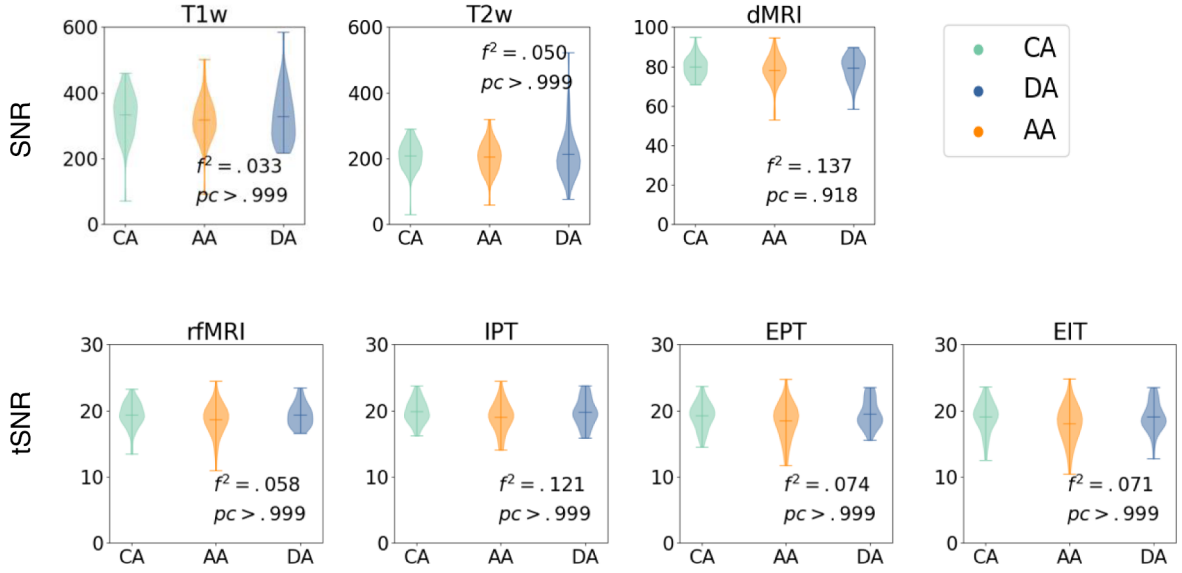

Fig. 5. Top row: SNR for T1w, T2w, and dMRI; bottom row: tSNR for fMRI (rfMRI, IPT, EPT and EIT). All measures are grouped by control, anxious and depressed subjects. We show p-values of F-test, and Cohen's f-square values. No significant group differences were observed (all corrected $p > .05$, corrected $\alpha = 0.007$). CA = Control Adolescents; DA = Depressed Adolescents; AA = Anxious Adolescents.

assessed using an emotional-dot-probe task[3](MacLeod et al., 1986; Mogg et al., 2000; Gotlib et al., 2004; Humphreys et al., 2016; see Supplemental 1). Administration of the NIH toolbox, Pennsylvania Computerized Neuropsychological Test Battery, and dot-probe tasks takes ~25mins, ~20mins, and ~15mins, respectively.

6. MRI quality and clinical factors

Head motion has been shown to differ between clinical and control populations, and to be associated with clinical symptom severity, in both child and adult samples (Kong et al., 2014; Yendiki et al., 2014; Couvy-Duchesne et al., 2016; Dosenbach et al., 2017). Here, we discuss relationships between estimates of SNR and participant motion with clinical labels and selected dimensional measures. Nearly half of our participants have reported difficulty holding still during the scanning session (see Fig. 2). Thus, we quantify associations of clinical factors with motion estimates and SNR.

Here, T1w and T2w structural images are processed in Freesurfer to obtain cortical and subcortical brain parcellations, brain masks, and surfaces. Diffusion MR images are corrected for EPI distortions using FSL's topup (Andersson et al., 2003) to compute susceptibility maps based on the $b = 0$ images obtained with opposite PE directions. This is combined with FSL's eddy (Andersson et al., 2016) to correct for eddy current distortions, motion, and EPI distortions. Functional MR images are corrected for motion using mcflirt (Jenkinson et al., 2002) and for EPI distortions using topup (Andersson et al., 2003) to compute susceptibility maps based on spin-echo images acquired with opposite PE directions. We correct each pair of AP- and PA-acquired rfMRI scans using spin-echo maps acquired before that pair of rfMRI scans (8 and 14 in Table 1); we correct the IPT fMRI scans using the spin-echo maps acquired before the last rfMRI scan (14 in Table 1). We correct the EPT and EIT fMRI scans using the last spin-echo maps, which are acquired

[3] We thank Katheryn Humphreys and Ian Gotlib for contributing the emotion-dot-probe task.

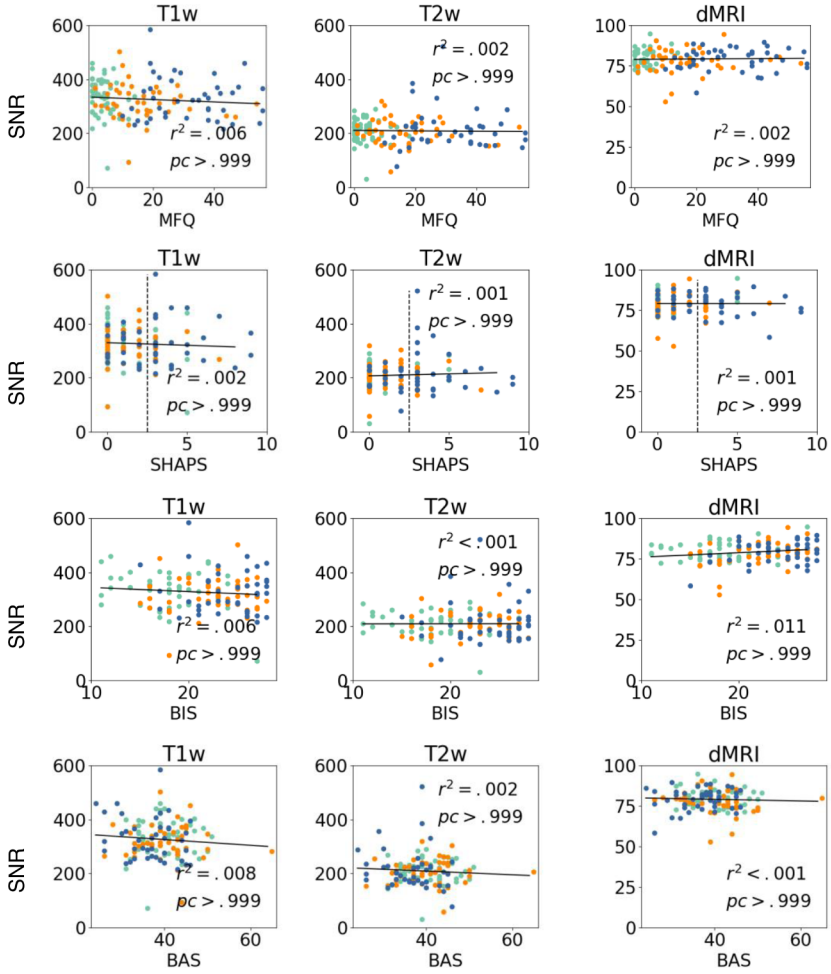

Fig. 6. SNR for T1w, T2w, and dMRI as a function of MFQ, SHAPS, BIS, and BAS. We show corrected p-values and r-squared values. No significant variable effects were observed (all corrected $p > .05$, corrected $\alpha = 0.001$).

before the EPT (20 in Table 1).

6.1. SNR

For structural and dMRI scans, SNR calculations use the region of interest (ROI) of the left unsegmented white matter from Freesurfer. The ROI is registered to the dMRI and T2 space using bbregister (Greve et al., 2009). The mean image intensity in this ROI is divided by the standard deviation of image intensities in a 20 mm^3 background ROI. The latter ROI does not contain any human tissue and is placed in the right-anterior-superior corner of the image. For fMRI we calculate temporal SNR (tSNR) for each voxel and average them. We show the average SNR obtained from the 4 dMRI scans and the average tSNR from all fMRI runs of the same scan (rfMRI: 4 runs; IPT: 2 runs; EPT: 2 runs; EIT: 4 runs).

6.1.1. Clinical group and SNR

Fig. 5 illustrates SNR for T1w, T2w, and dMRI, and tSNR for fMRI scans. We test for group differences using an F-test with multiple linear regression analysis of intercepts, with dependent variable of SNR and independent variables of clinical classification, age, and gender. Fig. 5 shows Cohen's f-square coefficient and Bonferroni corrected p-values, correcting for modalities and clinical classifications. No significant group differences are observed (all corrected $p > .05$, corrected $\alpha = 0.007$ for F-tests).

6.1.2. Clinical dimensions and SNR

In Fig. 6, we show SNR for T1w, T2w, and dMRI as a function of the continuous clinical variables (MFQ, SHAPS, and BIS-BAS). We perform a regression analysis with dependent variable of SNR and independent variables of continuous clinical scores, age, and gender. We fail to find significant relationships between SNR and the continuous scores after Bonferroni correction for multiple comparisons (all corrected $p > .05$, corrected $\alpha = 0.001$).

Fig. 7 shows the tSNR for the fMRI scans as a function of the same continuous clinical variables. No significant group differences are observed (all corrected $p > .05$, corrected $\alpha = 0.001$).

6.2. Motion

We estimate within-scan motion (i.e., average distance between vNavs from the same scan for T1w and T2w) and between scan motion (i.e., aggregate distance between different runs of scans) for each participant. Within-scan motion is assessed because this form of motion is known to impact data quality: e.g., corrupted k-space lines for structural, incorrect estimates of directional motion in dMRI, and spin history errors in fMRI. Between-scan motion may also impact analysis quality when combining different runs into a single analysis or processing steps such as surface reconstructions with Freesurfer.

FSL's FLIRT (Jenkinson et al., 2002) with 12 degrees of freedom is used to estimate within-scan motion parameters between TRs (navigator volumes). Mcflirt is used to estimate motion between consecutive volumes for fMRI. Eddy from FSL (Andersson et al., 2016) is used to

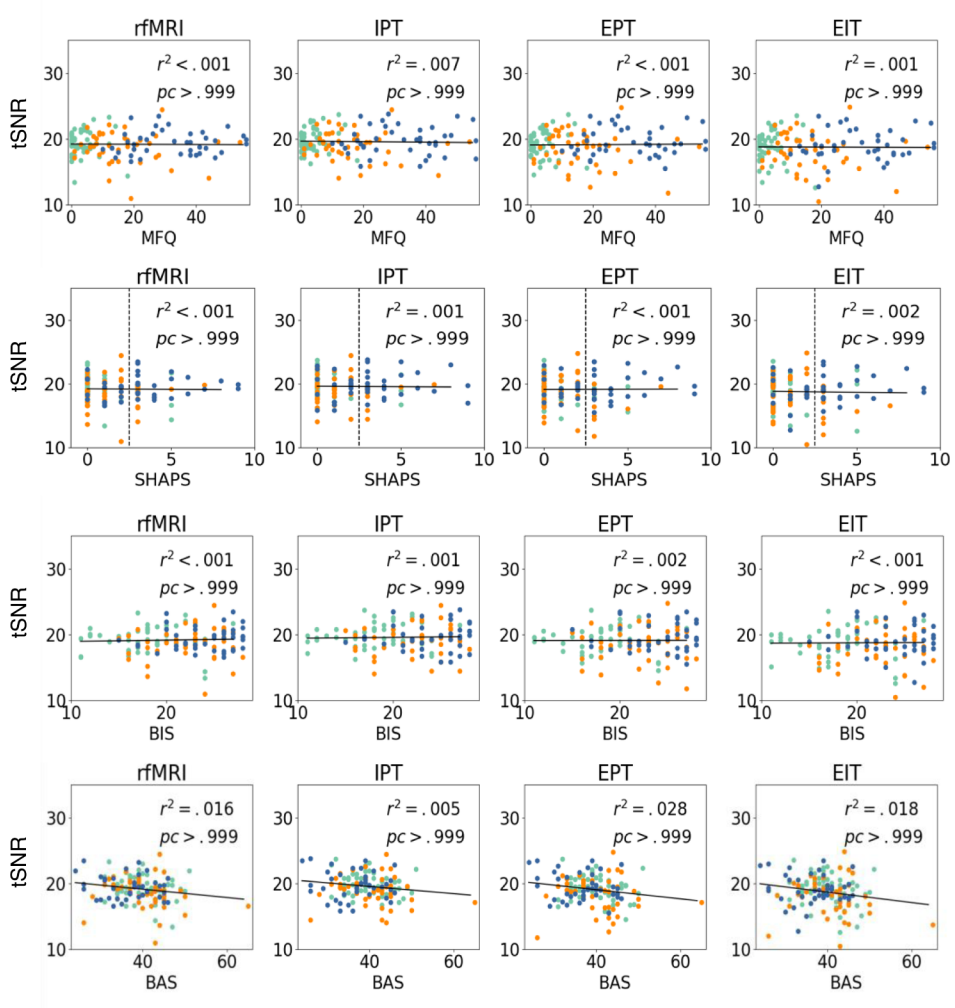

Fig. 7. tSNR for rfMRI, IPT, EPT, and EIT fMRI scans as a function of MFQ, SHAPS, BIS, and BAS. We show corrected p-values and r-squared values. No significant variable effects were observed (all corrected $p > .05$, corrected $\alpha = 0.001$).

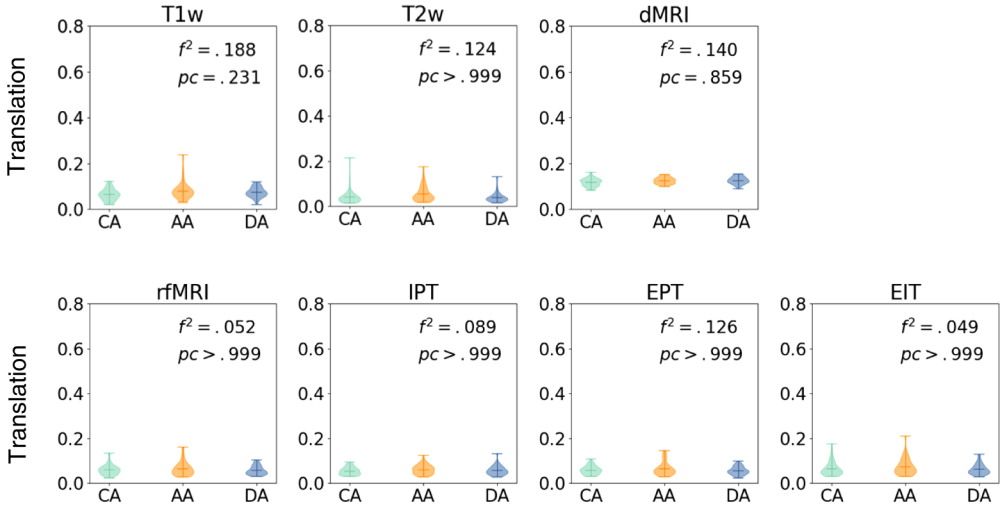

Fig. 8. Average translation within scans (voxels/sec). Motion measurements are shown per categorical group. We show p-values of F-test, and Cohen's f-square values. No significant group differences were observed (all corrected $p > .05$, corrected $\alpha = 0.007$). CA = Control Adolescents; DA = Depressed Adolescents; AA = Anxious Adolescents.

estimate motion within diffusion MRI volumes.

To detect which navigator volumes correspond to k-lines that should be thrown away and re-acquired, vNavs save in the dicom header their positions with respect to the first volume in quaternion format. Translation and rotation are calculated and, when differences are higher than half the voxel size, if the maximum number of re-acquisitions has not been reached, that volume is thrown away and re-acquired. The k-line to be re-acquired is always the one with highest motion. The vNav motion score s is calculated in millimeters as:

$$s = \sqrt{r^2 + 2\, r\, \|t - (t.\, u)u\| + \|t\|^2}, \quad \text{where} \quad r = 100\sqrt{2 - 2\cos(\alpha)}$$

and α is the rotation angle, $\boldsymbol{u}$ the rotation axis, and $\boldsymbol{t}$ the translation.

FLIRT is also used to estimate between-scan motion. For structural

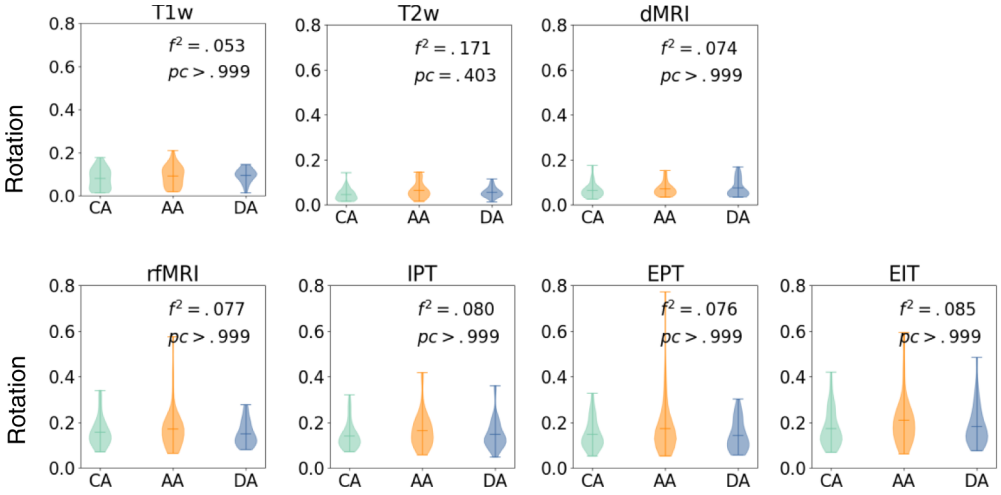

Fig. 9. Average rotation within scans (degrees/sec). Motion measurements are shown per categorical group. We show p-values of F-test, and Cohen's f-square values. No significant group differences were observed (all corrected $p > .05$, corrected $\alpha = 0.007$). CA = Control Adolescents; DA = Depressed Adolescents; AA = Anxious Adolescents.

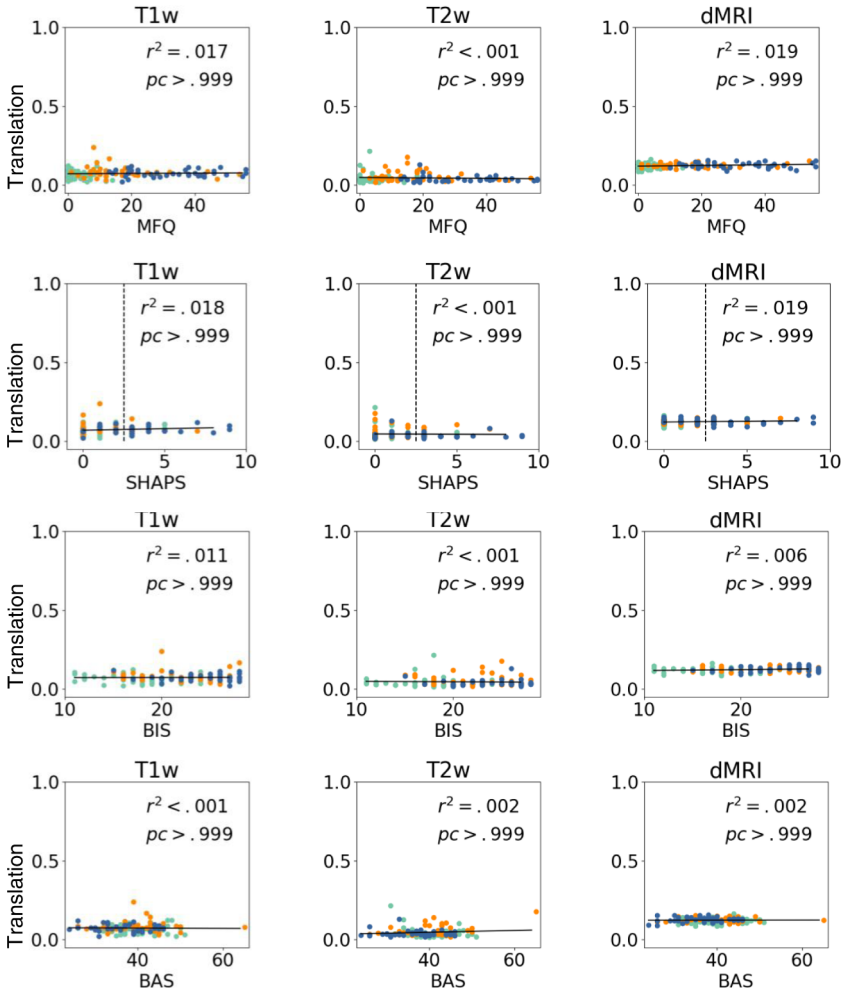

Fig. 10. Average translation within scans (voxels/sec). Scores are shown as a function of MFQ, SHAPS, BIS, and BAS. We show corrected p-values and r-squared values. No significant variable effects were observed (all corrected $p > .05$, corrected $\alpha = 0.001$).

images, FLIRT estimates motion parameter changes between the first navigator scans from the T1w and T2w images. For diffusion images, we estimate average motion parameter changes between the first b = 0 images of each of the 4 diffusion runs. Finally, for fMRI, we estimate motion parameter changes from the first volume of each task or rest run.

Framewise-displacement (FD; Power et al., 2012) is commonly used as scrubbing technique in fMRI and calculates the sum of absolute values of translational and rotational re-alignment estimates. Rotational estimates are converted from radians to millimeters by calculating the rotational trajectory in a sphere of 5 cm radius, an average distance from the center of an adult brain to the cortex. Root mean square (RMS) of FD across TRs (Siegel et al., 2014) is evaluated over fMRI scans to evaluate the number of TRs above a certain threshold.

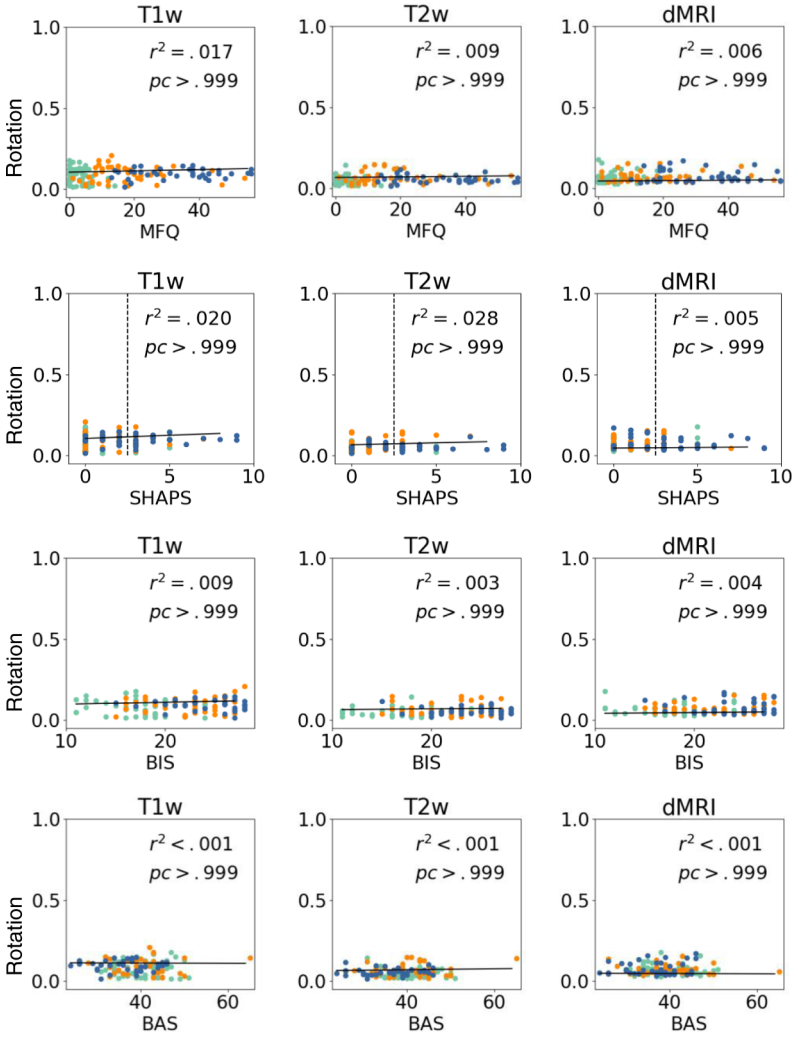

Fig. 11. Average rotation within scans (degrees/sec). Scores are shown as a function of MFQ, SHAPS, BIS, and BAS. We show corrected p-values and r-squared values. No significant variable effects were observed (all corrected $p > .05$, corrected $\alpha = 0.001$).

6.2.1. Motion estimates by group

Figs. 8 and 9 show average translation/rotation between TRs grouped by clinical category. We perform a T-test for each pair of groups and Bonferroni correction by categories and modalities. No significant group differences are observed (all corrected $p > .05$) for rotation or translation within scans. Rotation and translation between consecutive scans for each modality are shown in Supplemental Figures S1-S2.

6.2.2. Motion vs. clinical measures

Figs. 10 and 11 show average of rotation/translation between TRs as a function of continuous clinical variables (MFQ, SHAPS, and BIS-BAS) for structural and diffusion images. No significant variable effects are observed (all corrected $p > .05$). Fig. 10/Fig. 11 shows r-squared values and corrected p-values.

Figs. 12 and 13 show similar plots for fMRI scans. No significant variable effects are observed (all corrected $p > .05$, corrected $\alpha = 0.001$).

Plots of between-scan motion as a function of MFQ, SHAPS, and BIS-BAS are shown in Supplemental Figures S3-S4 for structural and diffusion scans, and in Supplemental Figures S5-S6 for functional scans. No significant variable effects are observed (all corrected $p > .05$, corrected $\alpha = 0.001$).

Fig. 14 shows the average percentage of volumes with FD > 0.9 mm, which has been used previously as a threshold for discarding fMRI volumes in adolescents (Siegel et al., 2014). Typically, when more than 20% of volumes surpass this threshold, the subject's scan is discarded from further analyses.

7. Harmonization

In this section we evaluate differences between the BANDA and HCP-D[4] data. To this end, we use 29 healthy controls from the BANDA dataset, and 29 age-matched adolescents from the HCP-D (17 females in HCP-D, 14 females in BANDA).

In Fig. 15 we show average SNR and tSNR for structural dMRI and rfMRI. We performed a paired T-test, with age and gender regressed out. We find no significant differences after Bonferroni correction for the number of modalities (all corrected $p > .05$, corrected $\alpha = 0.25$).

In Fig. 16 we show comparisons between the first two rfMRI scans. We did not include more rfMRI data because, for the HCP-D, the 4 runs were acquired in two different sessions, which could add potential confounds to comparisons. We preprocessed the first 2 rfMRI scans with FS-FAST (http://freesurfer.net/fswiki/FsFast), and performed a connectivity analysis seeding the bilateral isthmus, a primary region within the default mode network (Robinson et al., 2015; Seibert et al., 2011).

[4] We thank Dr. Leah Somerville and the HCP-D consortium for granting us early access to these data.

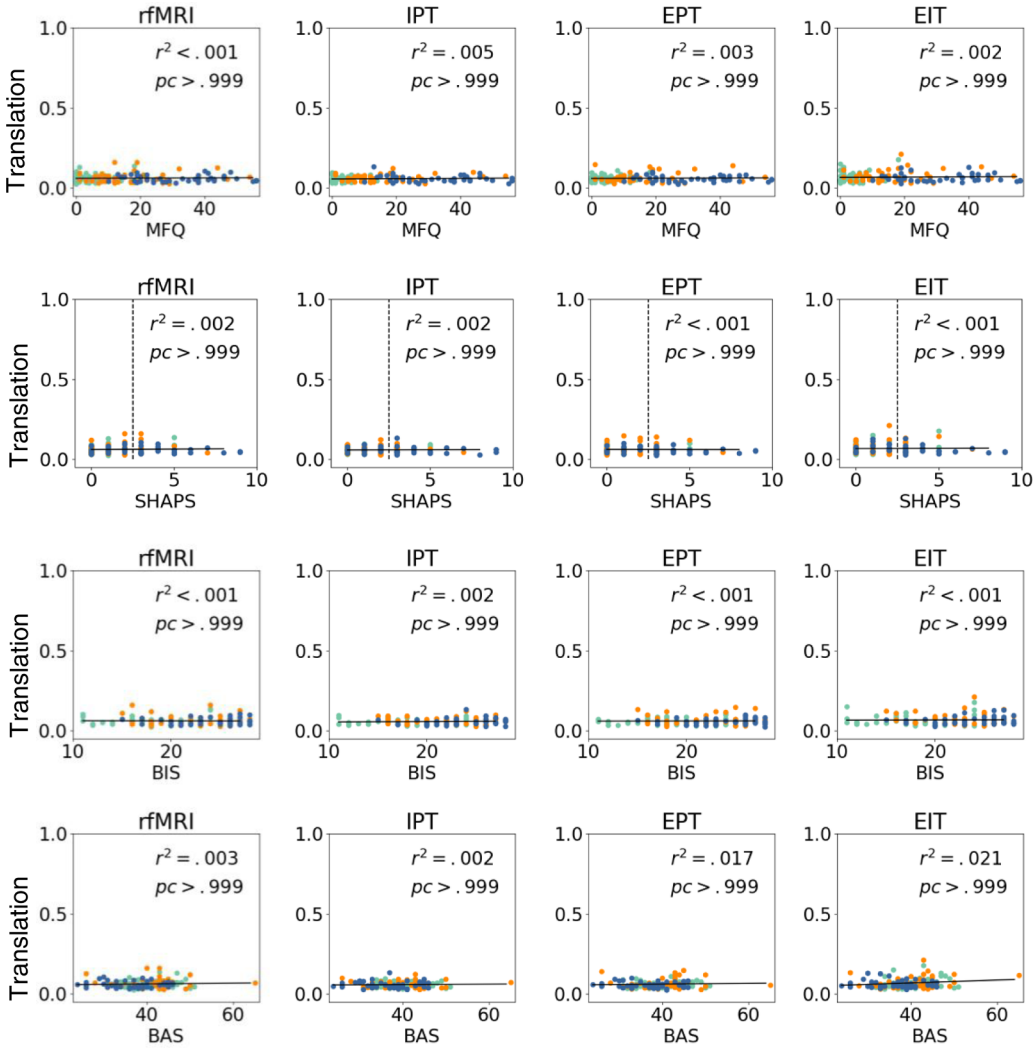

Fig. 12. Average translation within scans (voxels/sec). Scores are shown as a function of MFQ, SHAPS, BIS, and BAS. We show corrected p-values and r-squared values. No significant variable effects were observed (all corrected $p > .05$, corrected $\alpha = 0.001$).

We performed a One Sample Group Mean (OSGM) for BANDA (Fig. 16a) and HCP-D (Fig. 16b). For group analysis we performed a regression analysis with age and gender regressed out. Vertices that survived the significance threshold of $p > .01$ after surface-based permutation correction (Weiner et al., 2010; Greve et al., 2018) are shown in Fig. 16c.

Finally, to evaluate differences in dMRI, we ran bedpostx (Behrens et al., 2007; Jbabdi et al., 2012) with 3 anisotropic compartments on the full dMRI dataset. We evaluated the uncertainty of the main fiber orientation in regions where one fiber population is expected (i.e., corpus callosum, brainstem), and the volume fraction of each estimated anisotropic compartment in regions where more than one fiber population is expected (i.e., white matter that is 4 voxels away from the precuneus, and unsegmented white matter that is 4 voxels away from any other Freesurfer segmentation or parcellation label). Fig. 17 shows comparisons of these metrics between the BANDA and HCP-D datasets. We found no significant differences after performing T-tests with age and gender as regressors, and Bonferroni correction for the number of structures and anisotropic compartments (all $p > 0.05$).

8. Conclusion

The BANDA project provides a rich resource for researchers interested in understanding the neural correlates and predictors of adolescent depression and anxiety. Open-access imaging data include high-resolution T1w, T2w, dMRI with high-angular resolution, and fMRI with sub-second temporal resolution collected from anxious and depressed adolescents (ages 14–17), as well as their non-clinical counterparts. Consistent with the RDoC framework, the present project emphasizes sampling continuous symptom dimensions relevant to depression and anxiety, which will allow researchers to investigate relationships between neural and clinical diversity. Our QA analyses suggest high data quality with minimal influence of clinical classification or clinical features on SNR and motion estimates. Harmonization procedures discussed and analyses demonstrated here suggest confidence in allowing researchers to undertake joint analyses between data from BANDA and other relevant imaging projects.

Previous research has demonstrated associations between motion and clinical features that we present in our sample (e.g., Kong et al., 2014; Couvy-Duchesne et al., 2016; Dosenbach et al., 2017). Motion associated with clinical variables would be expected to bias imaging analyses aimed at better understanding these variables. In our data, QA analyses find mostly small and not statistically significant associations between clinical status or key clinical features and SNR or head motion estimates. Additionally, few functional imaging runs need to be discarded after the application of a motion censoring criterion (>20% of frames with >0.9 mm RMS of FD; see Siegel et al., 2014) and the majority of fMRI runs (i.e., 97.55%) are retained using this QA

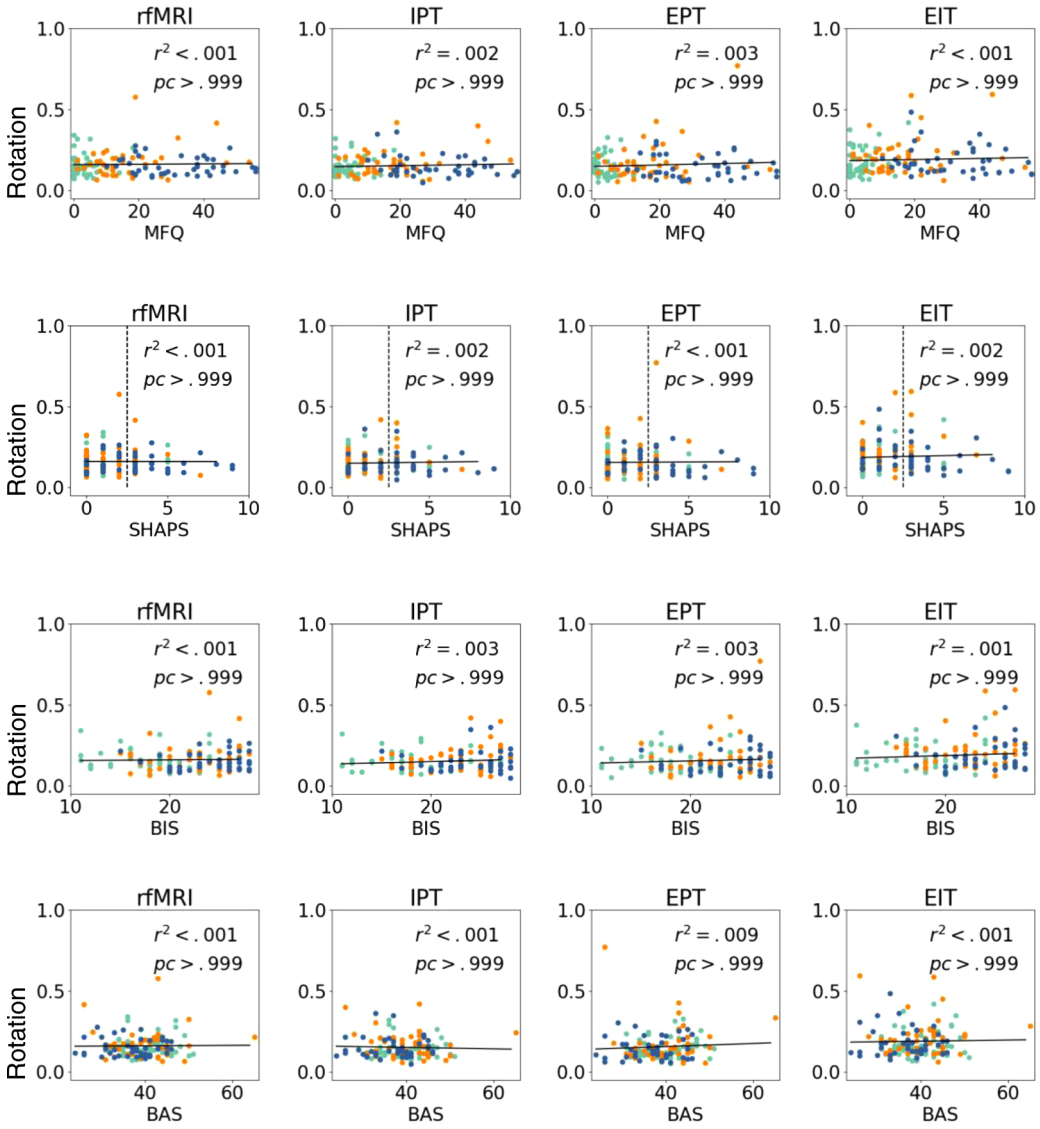

Fig. 13. Average rotation within scans (degrees/sec). Scores are shown as a function of MFQ, SHAPS, BIS, and BAS. We show corrected p-values and r-squared values. No significant variable effects were observed (all corrected ps $>$ 0.05, corrected $\alpha = 0.001$).

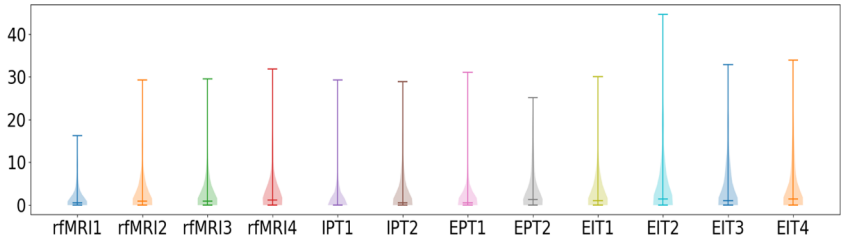

Fig. 14. Percentage of frames per subject with FD greater than 0.9 mm for each scan.

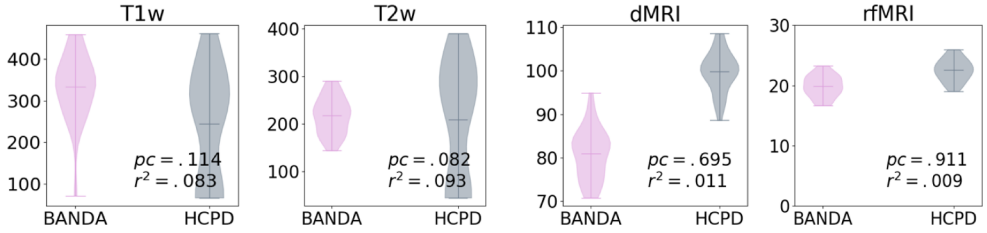

Fig. 15. Average SNR for dMRI, T1, and T2 images and tSNR for rfMRI. We show p-values of paired T-tests, and Cohen's f-square values. No significant group differences were observed (all corrected p $>$ .05, corrected $\alpha = 0.25$).

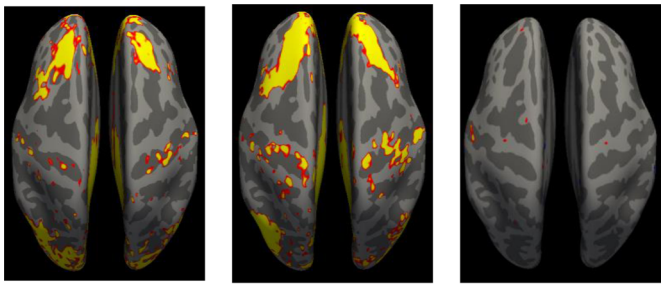

Fig. 16. One sample group mean analysis for BANDA (a) and HCP-D (b) at equal threshold. Results from regression analysis between BANDA and HCP-D are shown in (c) for vertices with $p > .01$ after permutation correction.

approach.

Harmonization of acquisition parameters and scanner hardware can help mitigate biases in joint analyses between independent MRI projects (e.g., Vollmar et al., 2010; Cercignani et al., 2003; Han et al., 2006; Jovicich et al., 2006; Leow et al., 2006; Friedman et al., 2008; Pardoe et al., 2008; Jovicich et al., 2009; Huppertz et al., 2010; Pagani et al., 2010; Yendiki et al., 2010; Fox et al., 2012; Magnotta et al., 2012; Jovicich et al., 2016; Palacios et al., 2017). Our scanner make and model, as well as dMRI and fMRI acquisition parameters, are harmonized with the HCP-D (Harms et al., 2018), CRHD-AA, and CRHD-DT. This should serve to minimize bias in joint analyses of connectomic measures derived from these projects. However, some acquisition differences do exist. These are mainly differences in head coil from the CRHD-DT, CRHD-DMS, and HCP-D, scanner make from the CRHD-DMS, and some structural acquisition parameters from all projects. Thus, additional analytic procedures may be beneficial for harmonizing BANDA data to these of other HCP projects. Several methods have been shown to be effective in reducing bias when comparing imaging data acquired from different sites with different hardware and acquisition parameters (Mirzaalian et al., 2016; Fortin et al., 2018; Yu et al., 2018; Karayumak et al., 2019), but travelling subjects or age- and gender-matched healthy subjects may need to be scanned at each harmonizing site. Comparisons of SNR, rfMRI connectivity analyses, and dMRI fiber compartment estimations between healthy adolescents from the BANDA and HCP-D cohorts have shown no significant differences, suggesting that a joint analysis at a larger scale would be feasible. However, interpretations of direct comparisons across different imaging studies may still need to be approached with caution (see Harms et al., 2018). More research is needed to understand the specific effects of protocol differences on imaging data. Although this was beyond the scope of the current project, more rigorous evaluation of acquisition differences may be undertaken by utilizing a travelling human phantom to provide potential correction factors for cross-study comparison.

Large imaging initiatives and harmonized protocols will allow analyses at larger scale with higher statistical power to potentially shed light into current psychiatric neuroimaging discrepancies (Murphy et al., 2011; Chen et al., 2016; Müller et al., 2017). Harmonization of independent neuroimaging projects may increase accuracy of prediction models of disease and treatment (e.g. Whitfield-Gabrieli et al., 2016). It is important to note that large imaging initiatives provide homogeneous clinical characterization definitions, which could exclude severe cases that would require personalized protocols. The outreach of such prediction models may be limited by clinical characterization definitions and exclusion criteria. Nevertheless, the BANDA project emphasized sampling the full spectrum of depressed/anxious symptoms and their comorbidity.

The BANDA project will provide the first HCP brain imaging dataset on adolescent anxiety and depression. Raw data and data minimally preprocessed with previously developed pipelines (Glasser et al., 2013) will be made publicly available. De-identified data will be available publicly through the NIMH Data Archive (https://ndar.nih.gov/). Future data will also be made available through this repository at regular intervals up to the planned total enrollment of 225 participants.

9. Author statement

V Siless: writing, visualization, validation, formal analysis, data curation, project administration, data collection, supervision, methodology; NA Hubbard: writing, supervision, project administration; R Jones: formal analysis, data collection, data curation; J Wang: data collection, data curation; N Lo: data curation; CCC Bauer: methodology; M Goncalves: data curation; IR Frosch: data collection, supervision, project administration; Daniel Norton: software; G Vergara: data collection; K Conroy: data collection; F Vaz De Souza: data collection; IM Rosso: conceptualization, validation, funding acquisition; A Hay: data collection, supervision; E Cosby: data collection; M Pinaire: data collection; Hirshfeld-Becker: conceptualization, data collection, supervision, funding acquisition; DA Pizzagalli: conceptualization, supervision, funding acquisition, project administration; A Henin: conceptualization, data collection, supervision, funding acquisition, project administration; DR.. SG Hofmann: conceptualization, supervision, funding acquisition, project administration; RP Auerbach: conceptualization, validation, funding acquisition, project administration; S Ghosh: conceptualization, methodology, validation, data curation, supervision, funding acquisition, project administration; JDE Gabrieli: conceptualization, project administration, supervision, funding acquisition; S Whitfield-Gabrieli: conceptualization, project administration, supervision, funding acquisition; A Yendiki: conceptualization, writing, project administration, data collection, supervision, methodology, funding acquisition.

10. Disclosures

Over the past three years, DAP received consulting fees from Akili Interactive Labs, BlackThorn Therapeutics, Boehringer Ingelheim, and Takeda Pharmaceuticals and an honorarium from Alkermes. SGH receives financial support from the Alexander von Humboldt Foundation and compensation for his work as editor from SpringerNature and the Association for Psychological Science. SGH also receives compensation for this role as an advisor from the Palo Alto Health Sciences and for his work as a Subject Matter Expert from John Wiley & Sons, Inc. and SilverCloud Health, Inc. No funding from these entities was used to support the current work, and all views expressed are solely those of the authors.

Acknowledgements

This project was supported by the National Institute of Mental Health, U01MH108168 (JDEG, SWG), and (F32MH114525 to NAH). AY was partially supported by R01EB021265 and U01EB026996. DAP was partially supported by R37MH068376 and R01MH101521. SSG was partially supported by R01EB020740 and P41EB019936. SGH was partly supported by R01AT007257, R01MH099021 and the James S. McDonnell Foundation. This project was made possible by the resources provided by Shared Instrumentation Grants 1S10RR023401, 1S10RR019307, and 1S10RR023043. The content is solely the responsibility of the authors and does not necessarily represent the official views of the National Institutes of Health or of any other sponsor.

Supplementary materials

Supplementary material associated with this article can be found, in the online version, at 10.1016/j.nicl.2020.102242.

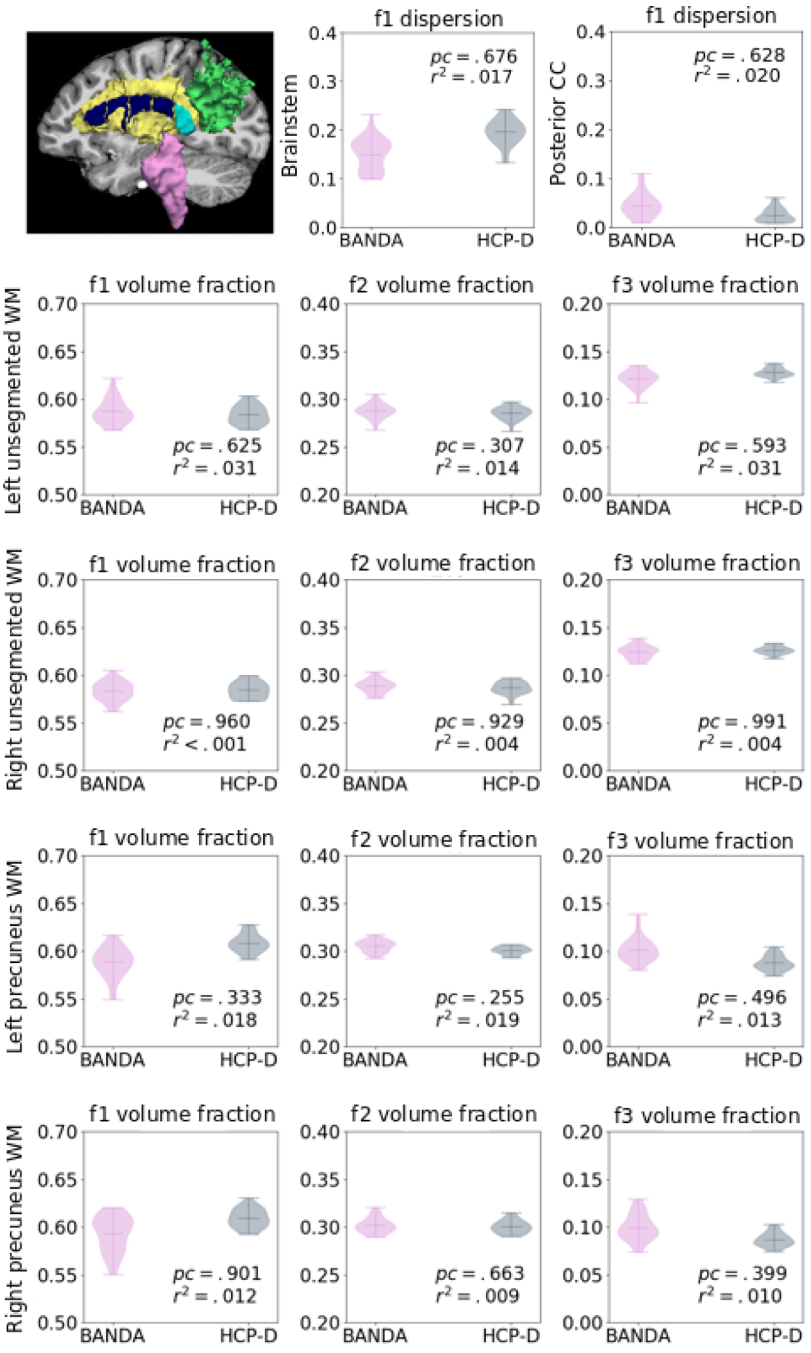

Fig. 17. Estimated uncertainty of the main anisotropic compartment in the posterior corpus callosum (CC; cyan), and brainstem (pink), and volume fractions of the all anisotropic compartments in unsegmented white matter (yellow) and precuneus white matter (green).

References

American Psychiatric Association, 2013. Diagnostic and Statistical Manual of Mental Disorders. American Psychiatric Associationhttps://doi.org/10.1176/appi.books.9780890425596.

Andersson, J.L.R., Skare, S., Ashburner, J., 2003. How to correct susceptibility distortions in spin-echo echo-planar images: application to diffusion tensor imaging. NeuroImage 20, 870–888. https://doi.org/10.1016/S1053-8119(03)00336-7.

Andersson, J.L.R., Sotiropoulos, S.N., 2016. An integrated approach to correction for off-resonance effects and subject movement in diffusion MR imaging. NeuroImage 125, 1063–1078. https://doi.org/10.1016/J.NEUROIMAGE.2015.10.019.

Angold, A., Costello, J., van Kämmen, W., Stouthamer-Loeber, M., 1996. Development of a short questionnaire for use in epidemiological studies of depression in children and adolescents: factor composition and structure across development. International Journal of Methods in Psychiatric Research 5, 251–262.

Barch, D.M., Burgess, Harms, G.C., Petersen, M.P., Schlaggar, S.E., Corbetta, B.L., Glasser, M., Curtiss, M.F., Dixit, S., Feldt, S., Nolan, C., Bryant, D., Hartley, E., Footer, T., Bjork, O., Poldrack, J.M., Smith, R., Johansen-Berg, S., Snyder, H., van Essen, A.Z., WU-Minn, D.C., Consortium, HCP, 2013. Function in the human connectome: task-fMRI and individual differences in behavior. NeuroImage 80, 169–189. https://doi.org/10.1016/j.neuroimage.2013.05.033.

Behrens, T.E.J., Berg, H.J., Jbabdi, S., Rushworth, M.F.S., Woolrich, M.W., 2007. Probabilistic diffusion tractography with multiple fibre orientations: What can we gain? NeuroImage 34, 144–155. https://doi.org/10.1016/j.neuroimage.2006.09.018.

Bookheimer, S.Y., Salat, D.H., Terpstra, M., Ances, B.M., Barch, D.M., Buckner, R.L., Burgess, G.C., Curtiss, S.W., Diaz-Santos, M., Elam, J.S., Fischl, B., Greve, D.N., Hagy, H.A., Harms, M.P., Hatch, O.M., Hedden, T., Hodge, C., Japardi, K.C., Kuhn, T.P., Ly, T.K., Smith, S.M., Somerville, L.H., Uğurbil, K., van der Kouwe, A., van Essen, D., Woods, R.P., Yacoub, E., 2019. The Lifespan Human Connectome Project in Aging: An overview. NeuroImage 185, 335–348. https://doi.org/10.1016/J.NEUROIMAGE.2018.10.009.

Bracht, T., Linden, D., Keedwell, P., 2015. A review of white matter microstructure alterations of pathways of the reward circuit in depression. Journal of Affective Disorders 187, 45–53. https://doi.org/10.1016/j.jad.2015.06.041.

Carver, C.S., White, T.L., 1994. Behavioral inhibition, behavioral activation, and affective responses to impending reward and punishment: The BIS/BAS Scales. Journal of Personality and Social Psychology 67, 319–333. https://doi.org/10.1037/0022-3514.67.2.319.

Casey, B.J., Cannonier, T., Conley, M.I., Cohen, A.O., Barch, D.M., Heitzeg, M.M., Soules, M.E., Teslovich, T., Dellarco, D.v., Garavan, H., Orr, C.A., Wager, T.D., Banich, M.T., Speer, N.K., Sutherland, M.T., Riedel, M.C., Dick, A.S., Bjork, J.M., Thomas, K.M., Chaarani, B., Mejia, M.H., Hagler, D.J., Daniela Cornejo, M., Sicat, C.S., Harms, M.P., Dosenbach, N.U.F., Rosenberg, M., Earl, E., Bartsch, H., Watts, R., Polimeni, J.R., Kuperman, J.M., Fair, D.A., Dale, A.M., 2018. The Adolescent Brain Cognitive Development (ABCD) study: Imaging acquisition across 21 sites. Developmental Cognitive Neuroscience 32, 43–54. https://doi.org/10.1016/J.DCN.2018.03.001.

Cercignani, M., Bammer, R., Sormani, M.P., Fazekas, F., Filippi, M., 2003. Inter-sequence and inter-imaging unit variability of diffusion tensor MR imaging histogram-derived metrics of the brain in healthy volunteers. American Journal of Neuroradiology 24, 638–643.

Cetin Karayumak, S., Bouix, S., Ning, L., James, A., Crow, T., Shenton, M., Kubicki, M., Rathi, Y., 2019. Retrospective harmonization of multi-site diffusion MRI data acquired with different acquisition parameters. NeuroImage 184, 180–200. https://doi.org/10.1016/j.neuroimage.2018.08.073.

Chai, X.J., Hirshfeld-Becker, D., Biederman, J., Uchida, M., Doehrmann, O., Leonard, J.A., Salvatore, J., Kenworthy, T., Brown, A., Kagan, E., de los Angeles, C., Whitfield-Gabrieli, S., Gabrieli, J.D.E., 2015. Functional and structural brain correlates of risk for major depression in children with familial depression. NeuroImage: Clinical 8, 398–407. https://doi.org/10.1016/j.nicl.2015.05.004.

Chen, G., Hu, X., Li, L., Huang, X., Lui, S., Kuang, W., Ai, H., Bi, F., Gu, Z., Gong, Q., 2016. Disorganization of white matter architecture in major depressive disorder: a meta-analysis of diffusion tensor imaging with tract- based spatial statistics. Nature Publishing Grouphttps://doi.org/10.1038/srep21825.

Clark, L.A., Watson, D., Reynolds, S., 1995. Diagnosis and Classification of Psychopathology: Challenges to the Current System and Future Directions. Annual Review of Psychology 46, 121–153. https://doi.org/10.1146/annurev.ps.46.020195.001005.

Couvy-Duchesne, B., Ebejer, J.L., Gillespie, N.A., Duffy, D.L., Hickie, I.B., Thompson, P.M., Martin, N.G., de Zubicaray, G.I., McMahon, K.L., Medland, S.E., Wright, M.J., 2016. Head Motion and Inattention/Hyperactivity Share Common Genetic Influences: Implications for fMRI Studies of ADHD. PloS one 11, e0146271. https://doi.org/10.1371/journal.pone.0146271.

Cullen, K.R., Klimes-Dougan, B., Muetzel, R., Mueller, B.A., Camchong, J., Houri, A., Kurma, S., Lim, K.O., 2010. Altered White Matter Microstructure in Adolescents With Major Depression: A Preliminary Study. Journal of the American Academy of Child and Adolescent Psychiatry. https://doi.org/10.1097/00004583-201002000-00011.

Delgado, M.R., Nystrom, L.E., Fissell, C., Noll, D.C., Fiez, J.A., 2000. Tracking the Hemodynamic Responses to Reward and Punishment in the Striatum. Journal of Neurophysiology 84, 3072–3077. https://doi.org/10.1152/jn.2000.84.6.3072.

di Martino, A., Yan, C.-G., Li, Q., Denio, E., Castellanos, F.X., Alaerts, K., Anderson, J.S., Assaf, M., Bookheimer, S.Y., Dapretto, M., Deen, B., Delmonte, S., Dinstein, I., Ertl-Wagner, B., Fair, D.A., Gallagher, L., Kennedy, D.P., Keown, C.L., Keysers, C., Lainhart, J.E., Lord, C., Luna, B., Menon, V., Minshew, N.J., Monk, C.S., Mueller, S., Müller, R.-A., Nebel, M.B., Nigg, J.T., O'Hearn, K., Pelphrey, K.A., Peltier, S.J., Rudie, J.D., Sunaert, S., Thioux, M., Tyszka, J.M., Uddin, L.Q., Verhoeven, J.S., Wenderoth, N., Wiggins, J.L., Mostofsky, S.H., Milham, M.P., 2014. The autism brain imaging data exchange: towards a large-scale evaluation of the intrinsic brain architecture in autism. Molecular psychiatry 19, 659–667. https://doi.org/10.1038/mp.2013.78.

Dosenbach, N.U.F., Koller, J.M., Earl, E.A., Miranda-Dominguez, O., Klein, R.L., Van, A.N., Snyder, A.Z., Nagel, B.J., Nigg, J.T., Nguyen, A.L., Wesevich, V., Greene, D.J., Fair, D.A., 2017. Real-time motion analytics during brain MRI improve data quality and reduce costs. NeuroImage 161, 80–93. https://doi.org/10.1016/j.neuroimage.2017.08.025.

Ducharme, S., Albaugh, M.D., Hudziak, J.J., Botteron, K.N., Nguyen, T.-V., Truong, C., Evans, A.C., Karama, S., Ball, W.S., Byars, A.W., Schapiro, M., Bommer, W., Carr, A., German, A., Dunn, S., Rivkin, M.J., Waber, D., Mulkern, R., Vajapeyam, S., Chiverton, A., Davis, P., Koo, J., Marmor, J., Mrakotsky, C., Robertson, R., McAnulty, G., Brandt, M.E., Fletcher, J.M., Kramer, L.A., Yang, G., McCormack, C., Hebert, K.M., Volero, H., Botteron, K., McKinstry, R.C., Warren, W., Nishino, T., Almli, C.R., Todd, R., Constantino, J., McCracken, J.T., Levitt, J., Alger, J., O'Neil, J., Toga, A., Asarnow, R., Fadale, D., Heinichen, L., Ireland, C., Wang, D.-J., Moss, E., Zimmerman, R.A., Bintliff, B., Bradford, R., Newman, J., Evans, A.C., Arnaoutelis, R., Pike, G.B., Collins, D.L., Leonard, G., Paus, T., Zijdenbos, A., Das, S., Fonov, V., Fu, L., Harlap, J., Leppert, I., Milovan, D., Vins, D., Zeffiro, T., van Meter, J., Lange, N., Froimowitz, M.P., Botteron, K., Almli, C.R., Rainey, C., Henderson, S., Nishino, T., Warren, W., Edwards, J.L., Dubois, D., Smith, K., Singer, T., Wilber, A.A., Pierpaoli, C., Basser, P.J., Chang, L.-C., Koay, C.G., Walker, L., Freund, L., Rumsey, J., Baskir, L., Stanford, L., Sirocco, K., Gwinn-Hardy, K., Spinella, G., McCracken, J.T., Alger, J.R., Levitt, J., O'Neill, J., 2014. Anxious/Depressed Symptoms are Linked to Right Ventromedial Prefrontal Cortical Thickness Maturation in Healthy Children and Young Adults. Cerebral Cortex 24, 2941–2950. https://doi.org/10.1093/cercor/bht151.

Fales, C.L., Barch, D.M., Rundle, M.M., Mintun, M.A., Snyder, A.Z., Cohen, J.D., Mathews, J., Sheline, Y.I., 2008. Altered Emotional Interference Processing in Affective and Cognitive-Control Brain Circuitry in Major Depression. Biological Psychiatry 63, 377–384. https://doi.org/10.1016/j.biopsych.2007.06.012.

Fergusson, D.M., Woodward, L.J., 2002. Mental Health, Educational, and Social Role Outcomes of Adolescents With Depression. Archives of General Psychiatry 59, 225. https://doi.org/10.1001/archpsyc.59.3.225.

Fortin, J.-P., Cullen, N., Sheline, Y.I., Taylor, W.D., Aselcioglu, I., Cook, P.A., Adams, P., Cooper, C., Fava, M., McGrath, P.J., McInnis, M., Phillips, M.L., Trivedi, M.H., Weissman, M.M., Shinohara, R.T., 2018. Harmonization of cortical thickness measurements across scanners and sites. NeuroImage 167, 104–120. https://doi.org/10.1016/J.NEUROIMAGE.2017.11.024.

Fox, R.J., Sakaie, K., Lee, J.C., Debbins, J.P., Liu, Y., Arnold, D.L., Melhem, E.R., Smith, C.H., Philips, M.D., Lowe, M., Fisher, E., 2012. A validation study of multicenter diffusion tensor imaging: Reliability of fractional anisotropy and diffusivity values. American Journal of Neuroradiology 33, 695–700. https://doi.org/10.3174/ajnr.A2844.

Friedman, L., Stern, H., Brown, G.G., Mathalon, D.H., Turner, J., Glover, G.H., Gollub, R.L., Lauriello, J., Lim, K.O., Cannon, T., Greve, D.N., Bockholt, H.J., Belger, A., Mueller, B., Doty, M.J., He, J., Wells, W., Smyth, P., Pieper, S., Kim, S., Kubicki, M., Vangel, M., Potkin, S.G., 2008. Test-retest and between-site reliability in a multi-center fMRI study. Human Brain Mapping 29, 958–972. https://doi.org/10.1002/hbm.20440.

Glasser, M.F., Smith, S.M., Marcus, D.S., Andersson, J.L.R., Auerbach, E.J., Behrens, T.E.J., Coalson, T.S., Harms, M.P., Jenkinson, M., Moeller, S., Robinson, E.C., Sotiropoulos, S.N., Xu, J., Yacoub, E., Ugurbil, K., van Essen, D.C., 2016. The Human Connectome Project's neuroimaging approach. Nature Neuroscience 19, 1175–1187. https://doi.org/10.1038/nn.4361.

Glasser, M.F., Sotiropoulos, S.N., Wilson, J.A., Coalson, T.S., Fischl, B., Andersson, J.L., Xu, J., Jbabdi, S., Webster, M., Polimeni, J.R., van Essen, D.C., Jenkinson, M., 2013. The minimal preprocessing pipelines for the Human Connectome Project. NeuroImage 80, 105–124. https://doi.org/10.1016/j.neuroimage.2013.04.127.

Gotlib, I.H., Krasnoperova, E., Yue, D.N., Joormann, J., 2004. Attentional Biases for Negative Interpersonal Stimuli in Clinical Depression. Journal of Abnormal Psychology 113, 127–135. https://doi.org/10.1037/0021-843X.113.1.121.

Greve, D.N., Fischl, B., 2018. False positive rates in surface-based anatomical analysis. NeuroImage 171, 6–14. https://doi.org/10.1016/j.neuroimage.2017.12.072.

Greve, D.N., Fischl, B., 2009. Accurate and robust brain image alignment using boundary-based registration. NeuroImage 48, 63–72. https://doi.org/10.1016/j.neuroimage.2009.06.060.

Gur, R., Ragland, J.D., Moberg, P.J., Turner, T.H., Bilker, W.B., Kohler, C., Siegel, S.J., Gur, R.E., 2001. Computerized Neurocognitive Scanning: I. Methodology and Validation in Healthy People. Neuropsychopharmacology 25, 766–776. https://doi.org/10.1016/S0893-133X(01)00278-0.

Han, X., Jovicich, J., Salat, D., van der Kouwe, A., Quinn, B., Czanner, S., Busa, E., Pacheco, J., Albert, M., Killiany, R., Maguire, P., Rosas, D., Makris, N., Dale, A., Dickerson, B., Fischl, B., 2006. Reliability of MRI-derived measurements of human cerebral cortical thickness: The effects of field strength, scanner upgrade and manufacturer. NeuroImage 32, 180–194. https://doi.org/10.1016/j.neuroimage.2006.02.051.

Hariri, A.R., Tessitore, A., Mattay, V.S., Fera, F., Weinberger, D.R., 2002. The amygdala response to emotional stimuli: A comparison of faces and scenes. NeuroImage 17, 317–323. https://doi.org/10.1006/nimg.2002.1179.

Harms, Michael P., Somerville, L.H., Ances, B.M., Andersson, J., Barch, D.M., Bastiani, M., Bookheimer, S.Y., Brown, T.B., Buckner, R.L., Burgess, G.C., Coalson, T.S., Chappell, M.A., Dapretto, M., Douaud, G., Fischl, B., Glasser, M.F., Greve, D.N., Hodge, C., Jamison, K.W., Jbabdi, S., Kandala, S., Li, X., Mair, R.W., Mangia, S., Marcus, D., Mascali, D., Moeller, S., Nichols, T.E., Robinson, E.C., Salat, D.H., Smith, S.M., Sotiropoulos, S.N., Terpstra, M., Thomas, K.M., Tisdall, M.D., Ugurbil, K., van der Kouwe, A., Woods, R.P., Zöllei, L., van Essen, D.C., Yacoub, E., 2018. Extending the Human Connectome Project across ages: Imaging protocols for the Lifespan Development and Aging projects. NeuroImage 183, 972–984. https://doi.org/10.1016/J.NEUROIMAGE.2018.09.060.

Henderson, S.E., Johnson, A.R., Vallejo, A.I., Katz, L., Wong, E., Gabbay, V., 2013. A preliminary study of white matter in adolescent depression: relationships with illness severity, anhedonia, and irritability. Frontiers in psychiatry 4, 152. https://doi.org/10.3389/fpsyt.2013.00152.

Hubbard, N., Siless, V., Frosch, I., Goncalves, M., Lo, N., Wang, J., Bauer, C., Conroy, K., Cosby, E., Hay, A., Jones, R., Pinaire, M., Vaz De Souza, F., Vergara, G., Ghosh, S., Henin, A., Hirshfeld-Becker, D., Hofmann, S., Rosso, I., Auerbach, R., Pizzagalli, D., Yendiki, A., Gabrieli, J., Whitfield-Gabrieli, S., 2020. Brain Function and Clinical Characterization in the Boston Adolescent Neuroimaging of Depression and Anxiety Study. NeuroImage: Clinical, 102240. https://doi.org/10.1016/j.nicl.2020.102240.

Humphreys, K.L., Kircanski, K., Colich, N.L., Gotlib, I.H., 2016. Attentional avoidance of fearful facial expressions following early life stress is associated with impaired social functioning. Journal of Child Psychology and Psychiatry and Allied Disciplines 57, 1174–1182. https://doi.org/10.1111/jcpp.12607.

Huppertz, H.J., Kröll-Seger, J., Klöppel, S., Ganz, R.E., Kassubek, J., 2010. Intra- and interscanner variability of automated voxel-based volumetry based on a 3D probabilistic atlas of human cerebral structures. NeuroImage 49, 2216–2224. https://doi.org/10.1016/j.neuroimage.2009.10.066.

Jbabdi, S., Sotiropoulos, S.N., Savio, A.M., Graña, M., Behrens, T.E.J., 2012. Model-based analysis of multishell diffusion MR data for tractography: How to get over fitting problems. Magnetic Resonance in Medicine 68, 1846–1855. https://doi.org/10.1002/mrm.24204.

Jenkinson, M., Bannister, P., Brady, M., Smith, S., 2002. Improved optimization for the robust and accurate linear registration and motion correction of brain images. NeuroImage 17, 825–841. https://doi.org/10.1016/S1053-8119(02)91132-8.

Jovicich, J., Czanner, S., Greve, D., Haley, E., van der Kouwe, A., Gollub, R., Kennedy, D., Schmitt, F., Brown, G., MacFall, J., Fischl, B., Dale, A., 2006. Reliability in multi-site structural MRI studies: Effects of gradient non-linearity correction on phantom and human data. NeuroImage 30, 436–443. https://doi.org/10.1016/j.neuroimage.2005.09.046.

Jovicich, J., Czanner, S., Han, X., Salat, D., van der Kouwe, A., Quinn, B., Pacheco, J., Albert, M., Killiany, R., Blacker, D., Maguire, P., Rosas, D., Makris, N., Gollub, R.,

Dale, A., Dickerson, B.C., Fischl, B., 2009. MRI-derived measurements of human subcortical, ventricular and intracranial brain volumes: Reliability effects of scan sessions, acquisition sequences, data analyses, scanner upgrade, scanner vendors and field strengths. NeuroImage 46, 177–192. https://doi.org/10.1016/j.neuroimage.2009.02.010.

Jovicich, J., Minati, L., Marizzoni, M., Marchitelli, R., Sala-Llonch, R., Bartrés-Faz, D., Arnold, J., Benninghoff, J., Fiedler, U., Roccatagliata, L., Picco, A., Nobili, F., Blin, O., Bombois, S., Lopes, R., Bordet, R., Sein, J., Ranjeva, J.P., Didic, M., Gros-Dagnac, H., Payoux, P., Zoccatelli, G., Alessandrini, F., Beltramello, A., Bargalló, N., Ferretti, A., Caulo, M., Aiello, M., Cavaliere, C., Soricelli, A., Parnetti, L., Tarducci, R., Floridi, P., Tsolaki, M., Constantinidis, M., Drevelegas, A., Rossini, P.M., Marra, C., Schönknecht, P., Hensch, T., Hoffmann, K.T., Kuijer, J.P., Visser, P.J., Barkhof, F., Frisoni, G.B., 2016. Longitudinal reproducibility of default-mode network connectivity in healthy elderly participants: A multicentric resting-state fMRI study. NeuroImage 124, 442–454. https://doi.org/10.1016/j.neuroimage.2015.07.010.

Kerestes, R., Davey, C.G., Stephanou, K., Whittle, S., Harrison, B.J., 2013. Functional brain imaging studies of youth depression: A systematic review☆ YNICL 4, 209–231. https://doi.org/10.1016/j.nicl.2013.11.009.

Kong, X.-Z., Zhen, Z., Li, X., Lu, H.-H., Wang, R., Liu, L., He, Y., Zang, Y., Liu, J., 2014. Individual differences in impulsivity predict head motion during magnetic resonance imaging. PloS one 9, e104989. https://doi.org/10.1371/journal.pone.0104989.

Krueger, R.F., 1999. The Structure of Common Mental Disorders. Archives of General Psychiatry 56, 921. https://doi.org/10.1001/archpsyc.56.10.921.

Lang, P.J., McTeague, L.M., Bradley, M.M., 2016. RDoC, DSM, and the reflex physiology of fear: A biodimensional analysis of the anxiety disorders spectrum. Psychophysiology 53, 336–347. https://doi.org/10.1111/psyp.12462.

Langner, O., Dotsch, R., Bijlstra, G., Wigboldus, D.H.J., Hawk, S.T., van Knippenberg, A., 2010. Presentation and validation of the Radboud faces database. Cognition and Emotion 24, 1377–1388. https://doi.org/10.1080/02699930903485076.

Leow, A.D., Klunder, A.D., Jack, C.R., Toga, A.W., Dale, A.M., Bernstein, M.A., Britson, P.J., Gunter, J.L., Ward, C.P., Whitwell, J.L., Borowski, B.J., Fleisher, A.S., Fox, N.C., Harvey, D., Kornak, J., Schuff, N., Studholme, C., Alexander, G.E., Weiner, M.W., Thompson, P.M., 2006. Longitudinal stability of MRI for mapping brain change using tensor-based morphometry. NeuroImage 31, 627–640. https://doi.org/10.1016/j.neuroimage.2005.12.013.

LeWinn, K.Z., Connolly, C.G., Wu, J., Drahos, M., Hoeft, F., Ho, T.C., Simmons, A.N., Yang, T.T., 2014. White Matter Correlates of Adolescent Depression: Structural Evidence for Frontolimbic Disconnectivity. Journal of the American Academy of Child & Adolescent Psychiatry 53, 899–909. https://doi.org/10.1016/j.jaac.2014.04.021.

Liao, M., Yang, F., Zhang, Y., He, Z., Su, L., Li, L., 2014. White matter abnormalities in adolescents with generalized anxiety disorder: A diffusion tensor imaging study. BMC Psychiatry 14, 41. https://doi.org/10.1186/1471-244X-14-41.

Luciana, M., Bjork, J.M., Nagel, B.J., Barch, D.M., Gonzalez, R., Nixon, S.J., Banich, M.T., 2018. Adolescent neurocognitive development and impacts of substance use: Overview of the adolescent brain cognitive development (ABCD) baseline neurocognition battery. Developmental Cognitive Neuroscience 32, 67–79. https://doi.org/10.1016/J.DCN.2018.02.006.

MacLeod, C., Mathews, A., Tata, P., 1986. Attentional Bias in Emotional Disorders. Journal of Abnormal Psychology. https://doi.org/10.1037/0021-843X.95.1.15.

MacMaster, F.P., Kusumakar, V., 2004. Hippocampal volume in early onset depression. BMC Medicine 2. https://doi.org/10.1186/1741-7015-2-2.

Magnotta, V.A., Matsui, J.T., Liu, D., Johnson, H.J., Long, J.D., Bolster, B.D., Mueller, B.A., Lim, K., Mori, S., Helmer, K.G., Turner, J.A., Reading, S., Lowe, M.J., Aylward, E., Flashman, L.A., Bonett, G., Paulsen, J.S., 2012. MultiCenter Reliability of Diffusion Tensor Imaging. Brain Connectivity 2, 345–355. https://doi.org/10.1089/brain.2012.0112.

Marrus, N., Belden, A., Nishino, T., Handler, T., Tilak Ratnanather, J., Miller, M., Barch, D., Luby, J., Botteron, K., 2015. Ventromedial prefrontal cortex thinning in preschool-onset depression. Journal of Affective Disorders 180, 79–86. https://doi.org/10.1016/j.jad.2015.03.033.

McClure, E.B., Monk, C.S., Nelson, E.E., Parrish, J.M., Adler, A., Blair, R.J.R., Fromm, S., Charney, D.S., Leibenluft, E., Ernst, M., Pine, D.S., 2007. Abnormal Attention Modulation of Fear Circuit Function in Pediatric Generalized Anxiety Disorder. Archives of General Psychiatry 64, 97. https://doi.org/10.1001/archpsyc.64.1.97.

Mirzaalian, H., Ning, L., Savadjiev, P., Pasternak, O., Bouix, S., Michailovich, O., Grant, G., Marx, C.E., Morey, R.A., Flashman, L.A., George, M.S., McAllister, T.W., Andaluz, N., Shutter, L., Coimbra, R., Zafonte, R.D., Coleman, M.J., Kubicki, M., Westin, C.F., Stein, M.B., Shenton, M.E., Rathi, Y., 2016. Inter-site and inter-scanner diffusion MRI data harmonization. NeuroImage 135, 311–323. https://doi.org/10.1016/J.NEUROIMAGE.2016.04.041.

Mogg, K., Millar, N., Bradley, B.P., 2000. Biases in eye movements to threatening facial expressions in generalized anxiety disorder and depressive disorder. Journal of abnormal psychology 109, 695–704.

Monk, C.S., Nelson, E.E., McClure, E.B., Mogg, K., Bradley, B.P., Leibenluft, E., Blair, R.J.R., Chen, G., Charney, D.S., Ernst, M., Pine, D.S., 2006. Ventrolateral Prefrontal Cortex Activation and Attentional Bias in Response to Angry Faces in Adolescents With Generalized Anxiety Disorder. American Journal of Psychiatry 163, 1091–1097. https://doi.org/10.1176/ajp.2006.163.6.1091.

Mugler, J.P., Bao, S., Mulkern, R.v., Guttmann, C.R.G., Robertson, R.L., Jolesz, F.A., Brookeman, J.R., 2000. Optimized Single-Slab Three-dimensional Spin-Echo MR Imaging of the Brain. Radiology 216, 891–899. https://doi.org/10.1148/radiology.216.3.r00au46891.

Mugler, John P, Brookeman, James R, 1990. Three-dimensional magnetization-prepared rapid gradient-echo imaging (3D MP RAGE). Magnetic Resonance in Medicine 15, 152–157. https://doi.org/10.1002/mrm.1910150117.

Müller, V.I., Cieslik, E.C., Serbanescu, I., Laird, A.R., Fox, P.T., Eickhoff, S.B., 2017. Altered brain activity in unipolar depression revisited: Meta-analyses of neuroimaging studies. JAMA Psychiatry 74, 47–55. https://doi.org/10.1001/jamapsychiatry.2016.2783.

Murphy, M.L., Frodl, T., 2011. Meta-analysis of diffusion tensor imaging studies shows altered fractional anisotropy occurring in distinct brain areas in association with depression. Biology of mood & anxiety disorders 1, 3. https://doi.org/10.1186/2045-5380-1-3.

Nichols, T.E., Das, S., Eickhoff, S.B., Evans, A.C., Glatard, T., Hanke, M., Kriegeskorte, N., Milham, M.P., Poldrack, R.A., Poline, J.-B., Proal, E., Thirion, B., van Essen, D.C., White, T., Yeo, B.T.T., 2017. Best practices in data analysis and sharing in neuroimaging using MRI. Nature Neuroscience 20, 299–303. https://doi.org/10.1038/nn.4500.

Pagani, E., Hirsch, J.G., Pouwels, P.J.W., Horsfield, M.A., Perego, E., Gass, A., Roosendaal, S.D., Barkhof, F., Agosta, F., Rovaris, M., Caputo, D., Giorgio, A., Palace, J., Marino, S., de Stefano, N., Ropele, S., Fazekas, F., Filippi, M., 2010. Intercenter differences in diffusion tensor MRI acquisition. Journal of Magnetic Resonance Imaging 31, 1458–1468. https://doi.org/10.1002/jmri.22186.

Palacios, E.M., Martin, A.J., Boss, M.A., Ezekiel, F., Chang, Y.S., Yuh, E.L., Vassar, M.J., Schnyer, D.M., MacDonald, C.L., Crawford, K.L., Irimia, A., Toga, A.W., Mukherjee, P., TRACK-TBI Investigators, 2017. Toward Precision and Reproducibility of Diffusion Tensor Imaging: A Multicenter Diffusion Phantom and Traveling Volunteer Study. AJNR. American journal of neuroradiology 38, 537–545. https://doi.org/10.3174/ajnr.A5025.

Pardoe, H., Pell, G.S., Abbott, D.F., Berg, A.T., Jackson, G.D., 2008. Multi-site voxel-based morphometry: Methods and a feasibility demonstration with childhood absence epilepsy. NeuroImage 42, 611–616. https://doi.org/10.1016/j.neuroimage.2008.05.007.

Peirce, J.W., 2008. Generating stimuli for neuroscience using PsychoPy. Frontiers in Neuroinformatics 2, 10. https://doi.org/10.3389/neuro.11.010.2008.

Peirce, J.W., 2007. PsychoPy—Psychophysics software in Python. Journal of Neuroscience Methods 162, 8–13. https://doi.org/10.1016/J.JNEUMETH.2006.11.017.

Peng, R.D., 2011. Reproducible Research in Computational Science. Science 334, 1226–1227. https://doi.org/10.1126/science.1213847.

Power, J.D., Barnes, K.A., Snyder, A.Z., Schlaggar, B.L., Petersen, S.E., 2012. Spurious but systematic correlations in functional connectivity MRI networks arise from subject motion. NeuroImage 59, 2142–2154. https://doi.org/10.1016/j.neuroimage.2011.10.018.

Reuter, M., Tisdall, M.D., Qureshi, A., Buckner, R.L., van der Kouwe, A.J.W., Fischl, B., 2015. Head motion during MRI acquisition reduces gray matter volume and thickness estimates. NeuroImage 107, 107–115. https://doi.org/10.1016/j.neuroimage.2014.12.006.

Robinson, M.E., Lindemer, E.R., Fonda, J.R., Milberg, W.P., Mcglinchey, R.E., Salat, D.H., 2015. Close-range blast exposure is associated with altered functional connectivity in Veterans independent of concussion symptoms at time of exposure. Human Brain Mapping 36, 911–922. https://doi.org/10.1002/hbm.22675.

Satterthwaite, T.D., Connolly, J.J., Ruparel, K., Calkins, M.E., Jackson, C., Elliott, M.A., Roalf, D.R., Hopson, R., Prabhakaran, K., Behr, M., Qiu, H., Mentch, F.D., Chiavacci, R., Sleiman, P.M.A., Gur, R.C., Hakonarson, H., Gur, R.E., 2016. The Philadelphia Neurodevelopmental Cohort: A publicly available resource for the study of normal and abnormal brain development in youth. NeuroImage 124, 1115–1119. https://doi.org/10.1016/j.neuroimage.2015.03.056.

Schmaal, L., Hibar, D.P., Sämann, P.G., Hall, G.B., Baune, B.T., Jahanshad, N., 2016. Cortical abnormalities in adults and adolescents with major depression based on brain scans from 20 cohorts worldwide in the ENIGMA Major Depressive Disorder Working Group. Nature Publishing Group 22, 900–909. https://doi.org/10.1038/mp.2016.60.

Schumann, G., Loth, E., Banaschewski, T., Barbot, A., Barker, G., Büchel, C., Conrod, P.J., Dalley, J.W., Flor, H., Gallinat, J., Garavan, H., Heinz, A., Itterman, B., Lathrop, M., Mallik, C., Mann, K., Martinot, J.-L., Paus, T., Poline, J.-B., Robbins, T.W., Rietschel, M., Reed, L., Smolka, M., Spanagel, R., Speiser, C., Stephens, D.N., Ströhle, A., Struve, M., 2010. The IMAGEN study: reinforcement-related behaviour in normal brain function and psychopathology. Molecular Psychiatry 15, 1128–1139. https://doi.org/10.1038/mp.2010.4.

Seibert, T.M., Brewer, J.B., 2011. Default network correlations analyzed on native surfaces. Journal of neuroscience methods 198, 301–311. https://doi.org/10.1016/j.jneumeth.2011.04.010.

Setsompop, K., Kimmlingen, R., Eberlein, E., Witzel, T., Cohen-Adad, J., McNab, J.A., Keil, B., Tisdall, M.D., Hoecht, P., Dietz, P., Cauley, S.F., Tountcheva, V., Matschl, V., Lenz, V.H., Heberlein, K., Potthast, A., Thein, H., van Horn, J., Toga, A., Schmitt, F., Lehne, D., Rosen, B.R., Wedeen, V., Wald, L.L., 2013. Pushing the limits of in vivo diffusion MRI for the Human Connectome Project. NeuroImage 80, 220–233. https://doi.org/10.1016/j.neuroimage.2013.05.078.

Siegel, J.S., Power, J.D., Dubis, J.W., Vogel, A.C., Church, J.A., Schlaggar, B.L., Petersen, S.E., 2014. Statistical improvements in functional magnetic resonance imaging analyses produced by censoring high-motion data points. Human Brain Mapping 35, 1981–1996. https://doi.org/10.1002/hbm.22307.

Smith, S.M., Beckmann, C.F., Andersson, J., Auerbach, E.J., Bijsterbosch, J., Douaud, G., Duff, E., Feinberg, D.A., Griffanti, L., Harms, M.P., Kelly, M., Laumann, T., Miller, K.L., Moeller, S., Petersen, S., Power, J., Salimi-Khorshidi, G., Snyder, A.Z., Vu, A.T., Woolrich, M.W., Xu, J., Yacoub, E., Uğurbil, K., van Essen, D.C., Glasser, M.F., 2013. Resting-state fMRI in the Human Connectome Project. NeuroImage 80, 144–168. https://doi.org/10.1016/j.neuroimage.2013.05.039.

Snaith, R.P., Hamilton, M., Morley, S., Humayan, A., Hargreaves, D., Trigwell, P., 1995. A scale for the assessment of hedonic tone. The Snaith-Hamilton Pleasure Scale. British

Journal of Psychiatry 167, 99–103. https://doi.org/10.1192/bjp.167.1.99.
Somerville, L.H., Bookheimer, S.Y., Buckner, R.L., Burgess, G.C., Curtiss, S.W., Dapretto, M., Elam, J.S., Gaffrey, M.S., Harms, M.P., Hodge, C., Kandala, S., Kastman, E.K., Nichols, T.E., Schlaggar, B.L., Smith, S.M., Thomas, K.M., Yacoub, E., van Essen, D.C., Barch, D.M., 2018. The Lifespan Human Connectome Project in Development: A large-scale study of brain connectivity development in 5–21 year olds. NeuroImage 183, 456–468. https://doi.org/10.1016/J.NEUROIMAGE.2018.08.050.
Stuhrmann, A., Suslow, T., Dannlowski, U., 2011. Facial emotion processing in major depression: A systematic review of neuroimaging findings. Biology of Mood and Anxiety Disorders. https://doi.org/10.1186/2045-5380-1-10.
Thomas, K.M., Drevets, W.C., Dahl, R.E., Ryan, N.D., Birmaher, B., Eccard, C.H., Axelson, D., Whalen, P.J., Casey, B.J., 2001. Amygdala Response to Fearful Faces in Anxious and Depressed Children. Archives of General Psychiatry 58, 1057–1063. https://doi.org/10.1001/archpsyc.58.11.1057.
Tisdall, M.D., Hess, A.T., Reuter, M., Meintjes, E.M., Fischl, B., van der Kouwe, A.J.W., 2012. Volumetric navigators for prospective motion correction and selective re-acquisition in neuroanatomical MRI. Magnetic resonance in medicine 68, 389–399. https://doi.org/10.1002/mrm.23228.
Tisdall, M.D., Reuter, M., Qureshi, A., Buckner, R.L., Fischl, B., van der Kouwe, A.J.W., 2016. Prospective motion correction with volumetric navigators (vNavs) reduces the bias and variance in brain morphometry induced by subject motion. NeuroImage 127, 11–22. https://doi.org/10.1016/j.neuroimage.2015.11.054.
Tottenham, N., Tanaka, J.W., Leon, A.C., McCarry, T., Nurse, M., Hare, T.A., Marcus, D.J., Westerlund, A., Casey, BJ J, Nelson, C., 2009. The NimStim set of facial expressions: Judgments from untrained research participants. Psychiatry Research 168, 242–249. https://doi.org/10.1016/j.psychres.2008.05.006.
Ugurbil, K., Xu, J., Auerbach, E.J., Moeller, S., Vu, A., Duarte-Carvajalino, J.M., Lenglet, C., Wu, X., Schmitter, S., Van de Moortele, P.F., Strupp, J., Sapiro, G., De Martino, F., Wang, D., Harel, N., Garwood, M., Chen, L., Feinberg, D.A., Smith, S.M., Miller, K.L., Sotiropoulos, S.N., Jbabdi, S., Andersson, J.L., Behrens, T.E., Glasser, M.F., Van Essen, D., Yacoub, E., 2013. Pushing spatial and temporal resolution for functional and diffusion MRI in the Human Connectome Project. Neuroimage 80, 80–104. https://doi.org/10.1016/j.neuroimage.2013.05.012.
van der Kouwe, A.J.W., Benner, T., Fischl, B., Schmitt, F., Salat, D.H., Harder, M., Sorensen, A.G., Dale, A.M., 2005. On-line automatic slice positioning for brain MR imaging. NeuroImage 27, 222–230. https://doi.org/10.1016/j.neuroimage.2005.03.035.
van Essen, D.C., Ugurbil, K., Auerbach, E., Barch, D., Behrens, T.E.J., Bucholz, R., Chang, A., Chen, L., Corbetta, M., Curtiss, S.W., della Penna, S., Feinberg, D., Glasser, M.F., Harel, N., Heath, A.C., Larson-Prior, L., Marcus, D., Michalareas, G., Moeller, S., Oostenveld, R., Petersen, S.E., Prior, F., Schlaggar, B.L., Smith, S.M., Snyder, A.Z., Xu, J., Yacoub, E., WU-Minn, HCP, Consortium, W.-M.H., 2012. The Human Connectome Project: a data acquisition perspective. NeuroImage 62, 2222–2231. https://doi.org/10.1016/j.neuroimage.2012.02.018.
Volkow, N.D., Koob, G.F., Croyle, R.T., Bianchi, D.W., Gordon, J.A., Koroshetz, W.J., Pérez-Stable, E.J., Riley, W.T., Bloch, M.H., Conway, K., Deeds, B.G., Dowling, G.J., Grant, S., Howlett, K.D., Matochik, J.A., Morgan, G.D., Murray, M.M., Noronha, A., Spong, C.Y., Wargo, E.M., Warren, K.R., Weiss, S.R.B., 2018. The conception of the ABCD study: From substance use to a broad NIH collaboration. Developmental Cognitive Neuroscience 32, 4–7. https://doi.org/10.1016/J.DCN.2017.10.002.
Vollmar, C., O'muircheartaigh, J., Barker, G.J., Symms, M.R., Thompson, P., Kumari, V., Duncan, J.S., Richardson, M.P., Koepp, M.J., 2010. Identical, but not the same: Intra-site and inter-site reproducibility of fractional anisotropy measures on two 3.0 T scanners. NeuroImage 51, 1384–1394. https://doi.org/10.1016/j.neuroimage.2010.03.046.
Vuilleumier, P., Armony, J.L., Driver, J., Dolan, R.J., 2001. Effects of Attention and Emotion on Face Processing in the Human Brain: An Event-Related fMRI Study. Neuron 30, 829–841. https://doi.org/10.1016/S0896-6273(01)00328-2.
Wechsler, D., 2011. Wechsler Abbreviated Scale of Intelligence, Second Edition (WASI-II). NCS Pearson, San Antonio, TX.
Weiner, M.W., 2010. Alzheimer's Disease Neuroimaging Initiative special issue. Neurobiology of Aging 31, 1259–1262. https://doi.org/10.1016/J.NEUROBIOLAGING.2010.05.006.
Whitfield-Gabrieli, S., Ghosh, S.S., Nieto-Castanon, A., Saygin, Z., Doehrmann, O., Chai, X.J., Reynolds, G.O., Hofmann, S.G., Pollack, M.H., Gabrieli, J.D.E., 2016. Brain connectomics predict response to treatment in social anxiety disorder. Molecular Psychiatry 21, 680–685. https://doi.org/10.1038/mp.2015.109.
Wojciulik, E., Kanwisher, N., Driver, J., 1998. Covert Visual Attention Modulates Face-Specific Activity in the Human Fusiform Gyrus: fMRI Study. Journal of Neurophysiology 79, 1574–1578. https://doi.org/10.1152/jn.1998.79.3.1574.
Woodward, L.J., Fergusson, D.M., 2001. Life course outcomes of young people with anxiety disorders in adolescence. Journal of the American Academy of Child and Adolescent Psychiatry 40, 1086–1093. https://doi.org/10.1097/00004583-200109000-00018.
Yendiki, A., Greve, D.N., Wallace, S., Vangel, M., Bockholt, J., Mueller, B.A., Magnotta, V., Andreasen, N., Manoach, D.S., Gollub, R.L., 2010. Multi-site characterization of an fMRI working memory paradigm: Reliability of activation indices. NeuroImage 53, 119–131. https://doi.org/10.1016/j.neuroimage.2010.02.084.
Yendiki, A., Koldewyn, K., Kakunoori, S., Kanwisher, N., Fischl, B., 2014. Spurious group differences due to head motion in a diffusion MRI study. NeuroImage 88, 79–90. https://doi.org/10.1016/j.neuroimage.2013.11.027.
Yu, M., Linn, K.A., Cook, P.A., Phillips, M.L., McInnis, M., Fava, M., Trivedi, M.H., Weissman, M.M., Shinohara, R.T., Sheline, Y.I., 2018. Statistical harmonization corrects site effects in functional connectivity measurements from multi-site fMRI data. Human brain mapping 39, 4213–4227. https://doi.org/10.1002/hbm.24241.